Check for updates

AGU ADVANCING EARTH AND SPACE SCIENCES

Water Resources Research

RESEARCH ARTICLE
10.1029/2023WR036719

Bedrock Controls on Water and Energy Partitioning

Robert S. Ehlert[1], W. Jesse Hahm[1], David N. Dralle[2], Daniella M. Rempe[3], and Diana M. Allen[4]

[1]Department of Geography, Simon Fraser University, Burnaby, BC, Canada, [2]Pacific Southwest Research Station, United States Forest Service, Davis, CA, USA, [3]Department of Geological Sciences, Jackson School of Geosciences, University of Texas at Austin, Austin, TX, USA, [4]Department of Earth Sciences, Simon Fraser University, Burnaby, BC, Canada

Key Points:

- Plant use of bedrock storage impacts water partitioning in seasonally dry climates
- In many parts of the western United States, root-zone storage deficits do not reset annually
- Plants may exhaust soil water storage and require bedrock water as early as April each year

Supporting Information:

Supporting Information may be found in the online version of this article.

Correspondence to:

R. S. Ehlert,
robert_ehlert@sfu.ca

Citation:

Ehlert, R. S., Hahm, W. J., Dralle, D. N., Rempe, D. M., & Allen, D. M. (2024). Bedrock controls on water and energy partitioning. *Water Resources Research*, *60*, e2023WR036719. https://doi.org/10.1029/2023WR036719

Received 16 NOV 2023
Accepted 25 JUL 2024

Abstract Across diverse biomes and climate types, plants use water stored in bedrock to sustain plant transpiration. Bedrock water storage ($S_{bedrock}$), in addition to soil moisture, thus plays an important role in water cycling and should be accounted for in the context of surface energy balances and streamflow generation. Yet, the extent to which bedrock water storage impacts hydrologic partitioning and influences latent heat fluxes has yet to be quantified at large scales. This is particularly important in Mediterranean climates, where the majority of precipitation is offset from energy delivery and plants must rely on water retained from the wet season to support summer growth. Here we present a simple and modified water balance approach to quantify the role of $S_{bedrock}$ on controlling hydrologic and energy partitioning. Specifically, we tracked evapotranspiration in excess of precipitation and mapped soil water storage capacity (S_{soil}, mm) across the western US in the context of Budyko's water partitioning framework. Our findings indicate that $S_{bedrock}$ is necessary to sustain plant transpiration across forests in the Sierra Nevada—some of the most productive forests on Earth—as early as April every year, which is counter to the current conventional thought that bedrock is exclusively used late in the dry season under extremely dry conditions. We found that the proportion of water that returns to the atmosphere would decrease dramatically without access to $S_{bedrock}$. When converted to latent heat energy, the median monthly flux associated with evapotranspiration of $S_{bedrock}$ can exceed 100 W/m^2 during the dry season.

Plain Language Summary Plants frequently use water stored in bedrock ($S_{bedrock}$) in order to grow. However, the proportion of precipitation that returns to the atmosphere (evapotranspiration) versus to streams (runoff), and the amount of latent heat—the energy associated with evaporating water—used as a result of access to $S_{bedrock}$ has not been measured. In Mediterranean climates, such as parts of the western US, the majority of energy (sunlight) is received during the dry season and plants must rely on water stored belowground during the wet season to sustain summer growth. In this study, we present two methods for calculating how much $S_{bedrock}$ influences the amount of water returning to the atmosphere versus streams and what that corresponds to in terms of latent heat energy at the surface. We use gridded data to compare the amount of water entering (precipitation) and exiting (evapotranspiration) the area and use a mapped soil water storage capacity product to draw conclusions about the timing and magnitude of plant transpiration that is a result of access to bedrock water. Our findings indicate that some of the Earth's most productive forests use $S_{bedrock}$ early in the growing season, consuming over 100 W/m^2 of latent heat energy in the summer.

1. Introduction

Globally, more precipitation (P) is returned to the atmosphere via evapotranspiration (ET) than is returned to the ocean via streamflow (Q) (Jasechko et al., 2013; Trenberth et al., 2007). Locally, precipitation partitioning between streamflow and evapotranspiration is mediated by climate. The relative magnitudes of the water balance components at a location are dictated by the availability of water supply (precipitation) versus demand (energy) (Budyko, 1974). Over long time frames, where change in storage (ΔS) can be considered negligible, the ratio of evapotranspiration relative to precipitation (i.e., the evaporative index, $\epsilon = ET/P = 1 - Q/P$) can be estimated based on the ratio of potential evapotranspiration (PET) relative to precipitation (the aridity index, $\Phi = PET/P$; see Table 1 for a list of variables and their definitions). In practice, most catchments fall near a single curve—the Budyko curve—when plotted in ET/P versus PET/P space. A number of parametric extensions have been proposed to the Budyko equation that account for seasonality (Feng et al., 2012; Hickel & Zhang, 2006; Xing et al., 2018), vegetation cover (Chen et al., 2013; Donohue et al., 2007; M. Liu et al., 2022; L. Zhang et al., 2001), subsurface storage dynamics (Milly, 1994a), and other catchment-specific characteristics (e.g., Choudhury, 1999; Lhomme & Moussa, 2016; H. Yang et al., 2014) and a general solution has been mathematically derived that

© 2024. The Author(s).
This is an open access article under the terms of the Creative Commons Attribution License, which permits use, distribution and reproduction in any medium, provided the original work is properly cited.

19447973, 2024, 8, Downloaded from https://agupubs.onlinelibrary.wiley.com/doi/10.1029/2023WR036719, Wiley Online Library on [21/08/2024]. See the Terms and Conditions (https://onlinelibrary.wiley.com/terms-and-conditions) on Wiley Online Library for rules of use; OA articles are governed by the applicable Creative Commons License

Table 1
Description of Referenced Variables

Variable	Dimensions	Description
A	L	Accumulated difference; calculated as $F_{out} - F_{in}$ over a given timeframe
ASI	(–)	Asynchronicity index
C	(–)	Snow cover
C_0	(–)	Snow cover threshold
$D_{\max}$	L	Maximum observed annual root-zone storage deficit; equivalent to minimum (annual) S_R
$D_{\min}$	L	Minimum observed root-zone storage deficit in a year
$D_{t_{n+1}}$	L	Root-zone storage deficit measured at time t_{n+1}
E_e	MT^{-3}	Latent heat flux associated with evapotranspiration sourced from bedrock water storage, expressed as power per unit area
ET	LT^{-1}	Evapotranspiration
ET_{obs}	LT^{-1}	Observed evapotranspiration
F_{in}	LT^{-1}	Inflow
F_{out}	LT^{-1}	Outflow
$MOY_{bedrock}$	(–)	Median month of year when bedrock water is needed to explain observed evapotranspiration
n	(–)	Variable used to quantify differences in the evaporative index for a particular aridity index, defined by (H. Yang et al., 2008)
P	LT^{-1}	Precipitation
P_{obs}	LT^{-1}	Observed precipitation
PET	LT^{-1}	Potential evapotranspiration
Q	LT^{-1}	Runoff (streamflow)
RR	(–)	Runoff ratio; calculated as $1 - \epsilon$
S	L	Running storage used to calculate $S_{bedrock(my)}$ which is constrained by zero and S_{soil}
$S_{bedrock}$	L	Bedrock water storage
$S_{bedrock(a)}$	L	Lower-bound maximum plant-available water storage capacity in bedrock when the deficit is reset annually, inferred from largest deficit in an average water year less mapped S_{soil}
$S_{bedrock(my)}$	L	Lower-bound maximum plant-available water storage capacity in bedrock when the deficit is not reset annually, inferred from total evapotranspiration that occurs after S_{soil} has been fully depleted
$S_{bedrock(my),month}$	L	Monthly (dry season) evapotranspiration sourced from bedrock water storage
$S_{\max}$	L	The minimum root-zone plant-available storage deficit, inferred from maximum deficit observed over entire time period of analysis
S_R	L	Median annual lower-bound root-zone storage deficit inferred from maximum deficit observed over a water year; equivalent to (annual) $D_{\max}$
S_{soil}	L	The maximum amount of plant-available water capable of being stored in the soil profile, from soils mapping
t	T	Time
ΔH_v	ML^2T^{-2}	Enthalpy of vaporization of water
ΔS	LT^{-1}	Change in storage
$\Delta\epsilon$	(–)	Relative difference between ϵ_{obs} and $\epsilon_{w/o\ bedrock}$
ϵ	(–)	Evaporative index; calculated as ET/P
ϵ_{obs}	(–)	Observed evaporative index; calculated as ET_{obs}/P_{obs}
$\epsilon_{w/o\ bedrock}$	(–)	Observed evaporative index without bedrock water storage; calculated as ϵ_{obs} $(ET_{obs} - S_{bedrock(my)}/P_{obs})$
ρ_w	$L^{-3}M$	Density of water
Φ	(–)	Aridity index; calculated as PET/P

19447973, 2024, 8, Downloaded from https://agupubs.onlinelibrary.wiley.com/doi/10.1029/2023WR036719, Wiley Online Library on [21/08/2024]. See the Terms and Conditions (https://onlinelibrary.wiley.com/terms-and-conditions) on Wiley Online Library for rules of use; OA articles are governed by the applicable Creative Commons License

captures the catchment characteristics in a single parameter (H. Yang et al., 2008). The relationship described by Budyko also emerges from process-based hydrological models (e.g., Donohue et al., 2012; Entekhabi & Rodriguez-Iturbe, 1994; Feng et al., 2015; B. Fu, 1981; Porporato et al., 2004, etc.).

It is well documented that catchments with asynchronous climates, defined as climates where the majority of precipitation is temporally offset from energy delivery (Feng et al., 2019; Klos et al., 2018), are not well represented by the Budyko framework (e.g., J. Fu & Wang, 2019; Viola et al., 2017). These deviations can be reduced by incorporating catchment characteristics that account for vadose zone dynamics (e.g., Milly, 1994a; Sposito, 2017), precipitation seasonality (e.g., J. Fu & Wang, 2019), groundwater-dependent *ET* (e.g., Wang & Zhou, 2016) and storage changes (e.g., Condon & Maxwell, 2017), and subsurface critical zone structure (Hahm et al., 2019). Yet, there have been no attempts to quantify the extent to which bedrock water storage alters annual hydrologic partitioning at large scales, even though a substantial proportion of plant transpiration is sourced from bedrock water storage ($S_{bedrock}$) in asynchronous climates (e.g., Hahm et al., 2020; Hubbert et al., 2001; Witty et al., 2003).

The gap in knowledge surrounding $S_{bedrock}$ dynamics is not limited to hydrologic partitioning. Both global circulation models (GCMs) and dynamic global vegetation models (DGVMs) typically do not parameterize rock moisture as, historically, it has been difficult to quantify at large-scales. In asynchronous climates, DGVMs have been shown to struggle predicting dry-season plant transpiration and growth (Hickler et al., 2006, 2012) while GCMs fall short when predicting extreme precipitation and temperature (Tsaknias et al., 2016). After accounting for bedrock water, Lapides et al. (2024) found that LPJ-GUESS, a commonly used DGVM, was able to more accurately capture observed behaviors in the Northern California Coast Ranges. To our knowledge, there have been no attempts to close this gap in GCMs for the purpose of modeling latent heat flux—the transfer of heat between the terrestrial biosphere and atmosphere. Relying on soil moisture dynamics to explain latent heat flux patterns may be sufficient in humid climates, where the availability of atmospheric water vapor is less limiting, but it accounts poorly for climates that rely on water stored deep in the subsurface to compensate for a lack of precipitation during the summer dry season. It stands to reason that bedrock water storage, in addition to soil moisture, is necessary to evaluate land energy budgets. Given that soil moisture content has been shown to influence extreme daily temperatures (Durre et al., 2000), regulate the number of large fires (Jensen et al., 2018) and length of the wildfire season (Rakhmatulina et al., 2021), and was a contributing factor to the 2003 record-breaking heat wave in Europe (Fischer et al., 2007), the integration of $S_{bedrock}$ into GCMs could drastically shift predictions in asynchronous climates.

Early approaches for estimating subsurface storage deficits, calculated by taking the difference between precipitation and evaporation over time, date back to at least the 1960s (Grindley, 1960, 1968). In the literature, these methods were used mostly to estimate groundwater recharge (e.g., Finch, 2001; Rushton & Ward, 1979; Rushton et al., 2006, etc.) and were limited by spatial and temporal data resolution. More recently, remotely sensed water fluxes have been used to estimate root-zone storage deficits (S_R) at large scales. For example, continental-scale S_R has been estimated using mass balance approaches (e.g., de Boer-Euser et al., 2016; Gao et al., 2014; Stocker et al., 2023) and a methodology for estimating S_R at a global scale has been proposed by Wang-Erlandsson et al. (2016), and extended to account for snow cover by Dralle et al. (2021), which has been used to investigate ecosystem resilience (Singh et al., 2022), plant water-use sensitivity resulting from interannual rainfall variability (Dralle et al., 2020), and drought coping mechanisms in rainforest-savanna transects (Singh et al., 2020). Existing field-scale measurements (e.g., Rempe & Dietrich, 2018), which cannot be extrapolated over larger scales due to the spatial heterogeneity of plant rooting structures across different climates soil types and bedrock weathering patterns (Gentine et al., 2012; Sivandran & Bras, 2013), align well with satellite-derived S_R (McCormick et al., 2021). Root-zone storage deficits calculated via the deficit method influence the proportion of precipitation that returns to the atmosphere, for a given aridity index, in Australian catchments (Cheng et al., 2022). When combined with existing soil water storage capacity data sets (e.g., Gridded National Soil Survey Geography Database (gNATSGO); Survey Staff, 2019), satellite-derived S_R has been used to estimate $S_{bedrock}$ for the contiguous United States (McCormick et al., 2021).

In this study, we examine the extent to which the bedrock root-zone, which extends beneath the typically thin (<1 m) soil profile, influences water and energy budgets in the western US. More specifically, we investigate how plant access to bedrock water controls water partitioning and latent heat fluxes. We use a simple water balance approach combined with a national soil coverage database (i.e., gNATSGO), gridded water flux data, and a recent

19447973, 2024, 8, Downloaded from https://agupubs.onlinelibrary.wiley.com/doi/10.1029/2023WR036719, Wiley Online Library on [21/08/2024]. See the Terms and Conditions (https://onlinelibrary.wiley.com/terms-and-conditions) on Wiley Online Library for rules of use; OA articles are governed by the applicable Creative Commons License

data set of gridded subsurface water storage capacity to provide insights regarding the transfer of water from bedrock to the atmosphere. We then use an alternative mass-balance approach that allows for inter-annual deficit accrual and S_{soil} prioritization to corroborate the water balance inferences of annual evapotranspiration that is attributed to access to bedrock water reserves. Finally, we use this method to quantify lower-bounds on the amount of annual evapotranspiration accessed from the bedrock root-zone, infer the influence of $S_{bedrock}$ on hydrologic and energy partitioning properties, and show that plant transpiration in many parts of the western US relies on bedrock water early into the growing season, counter to conventional understanding that bedrock is used only late in the dry season.

In providing a simple, reproducible framework for quantifying the impacts of $S_{bedrock}$ on hydrologic and energy partitioning we look to answer three questions: (a) How early into the growing season do plants in asynchronous climates rely on $S_{bedrock}$ to sustain summer growth?; (b) How does access to bedrock water impact the partitioning of precipitation into evapotranspiration versus streamflow?; and (c) What is the latent heat flux associated with plant use of bedrock water?

2. Methods

To assess bedrock controls on water and energy partitioning, we apply two approaches: (a) an annual water balance, which calculates the total inferred annual evapotranspiration sourced from bedrock by tracking incoming and outgoing water fluxes; and (b) a non-resetting deficit model, which modifies the annual water balance model to account for multi-year deficit accrual and prioritizes S_{soil} use. To differentiate between the models, we use the nomenclature $S_{bedrock(a)}$ when referring to the model using an annual resetting deficit and $S_{bedrock(my)}$ when referring to the multi-year deficit accrual method. The annual water balance method provides conservative, lower-bound constraints on bedrock water use based on conservation of mass, while the non-resetting deficit model accounts for multi-year deficit accrual and better represents the full-scale of long-term subsurface storage dynamics.

In both cases, gridded timeseries of water flux data, in combination with an existing soil water capacity data set (gNATSGO), are used to estimate the median annual evapotranspiration sourced from bedrock. However, the input variables of the models differ. The annually resetting water balance method tracks incoming (precipitation) and outgoing (evapotranspiration) fluxes, at a pixel scale, to determine the amount of evapotranspiration that can be attributed to bedrock (i.e., *ET* in excess of soil water storage during dry periods) in a typical water year. The long-term deficit method is a similar mass-balance approach that instead tracks deficit throughout the entire study period as opposed to on an annual basis (Figure 1). The result represents an alternative method to calculating $S_{bedrock}$ that takes into consideration deep bedrock reserves that may be unaccounted for by assuming a resetting deficit. We then use the latter method to separate the western contiguous US into three categories of varying degrees of deficit accrual over the study period (Figure 2). Finally, we investigate the timing of bedrock water use in the growing season and calculate the latent heat energy used to explore the role of plant use of bedrock water on land surface energy fluxes.

2.1. Study Area

We restricted our study area to winter-wet, summer-dry climate regions of the western contiguous US. To identify these climate regions, we use the asynchronicity index (*ASI*, (Feng et al., 2019)) calculated from monthly TerraClimate precipitation and potential evapotranspiration values (Abatzoglou et al., 2018). We limited the study domain to pixels with an asynchronicity index greater than or equal to 0.40. This is a slightly stricter threshold (0.36) than proposed by Feng et al. (2019) to designate Mediterranean climates as we found 0.36 included parts of the southwest that are typically classified as semi-arid or desert using the Köppen-Geiger climate classification (Kottek et al., 2006). The masked coverage of the contiguous US, as well as computed asynchronicity index values, are shown in Figure S1 of the Supporting Information S1.

We additionally masked out pixels where:

1. Long-term evapotranspiration exceeds precipitation, for example, due to irrigated agricultural lands or data error;
2. Land cover (via NLCD) that is not classified as evergreen, deciduous, mixed forest or shrub/scrub (see Figure S14 in Supporting Information S1);

19447973, 2024, 8, Downloaded from https://agupubs.onlinelibrary.wiley.com/doi/10.1029/2023WR036719, Wiley Online Library on [21/08/2024]. See the Terms and Conditions (https://onlinelibrary.wiley.com/terms-and-conditions) on Wiley Online Library for rules of use; OA articles are governed by the applicable Creative Commons License

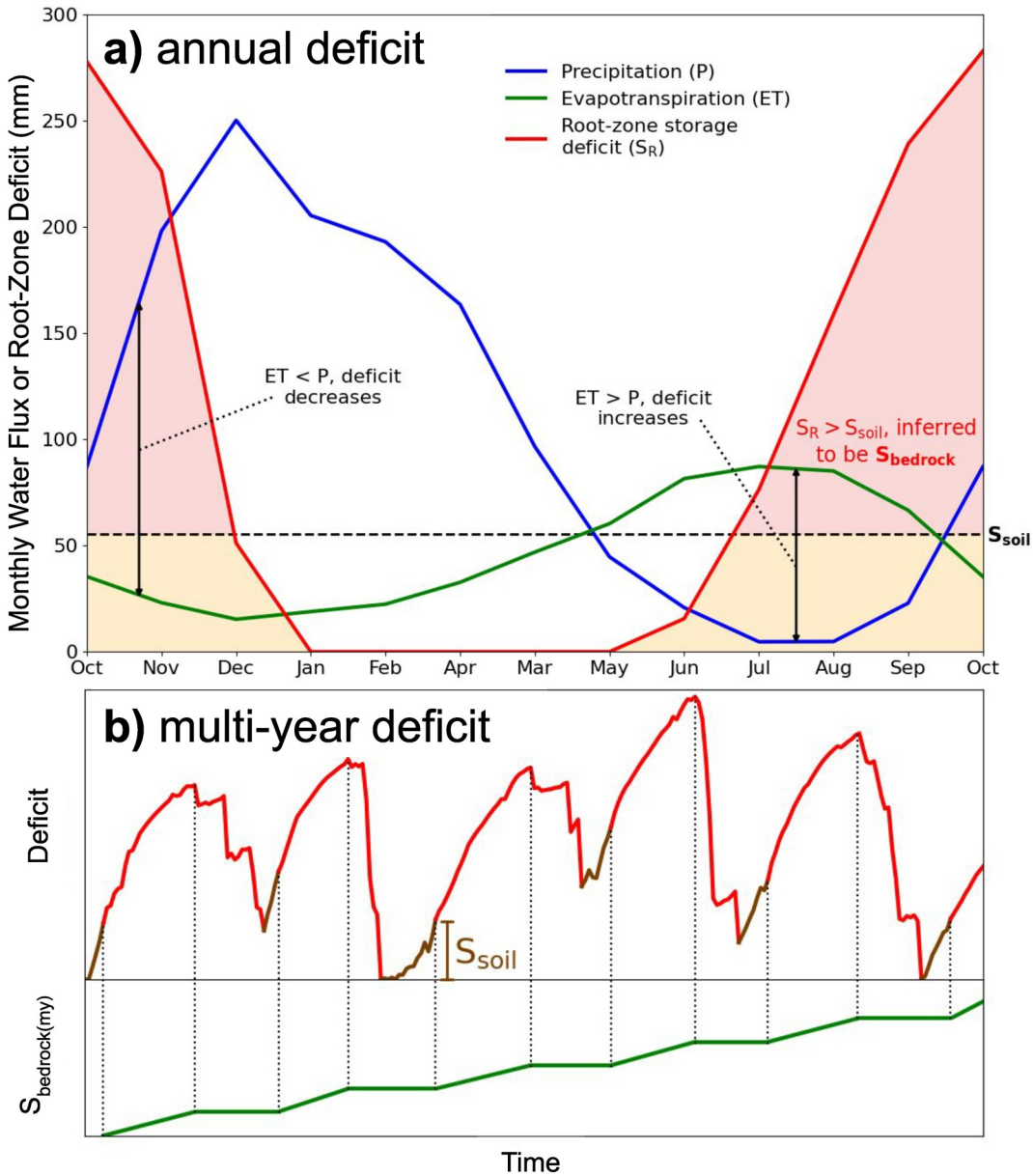

Figure 1. (a) Conceptual diagram describing the root-zone storage deficit characteristics of a typical water year (October 1–September 30) in asynchronous climates. At the beginning of the wet season, the deficit accrued during the dry season begins to decrease as $P > ET$. Prior to the beginning of the following dry season, the deficit returns to zero and remains at, or near, zero until $ET > P$. When ET remains $>P$ such that the deficit surpasses the soil water storage capacity (S_{soil}), plant transpiration is inferred to be a result of access to water stored below the soil layer, that is, $S_{bedrock}$. Figure is adapted from Lapides, Hahm, Rempe, Whiting, and Dralle (2022), Figure 1d. (b) Process outlining pixel-scale $S_{bedrock(my)}$ (green) accumulation under a non-resetting deficit. ET prioritizes the use of S_{soil} (brown; representing maximum pixel-level soil water holding capacity) when available and incoming P preferentially refills S_{soil} prior to $S_{bedrock(my)}$. As before, the root-zone storage deficit (red) grows during the dry-season and decreases during the wet-season but, during extended drought periods, may not fully replenish every year. $S_{bedrock(my)}$ grows as a step-function only when ET exceeds water stored in soil.

3. Soil water storage data sets (i.e., gNATSGO) do not have spatial coverage; or
4. Underlying bedrock is greater than 1.5 m (via gNATSGO) from the surface.

For this process, we use a gridded climate product from point observations (Parameter-elevation Regressions on Independent Slopes Model (PRISM); C. Daly et al., 2015), the Penman-Monteith-Leuning (PML) ET product (Y. Zhang et al., 2019), the Normalized Difference Snow Index (NDSI) (Hall et al., 2016), the United States

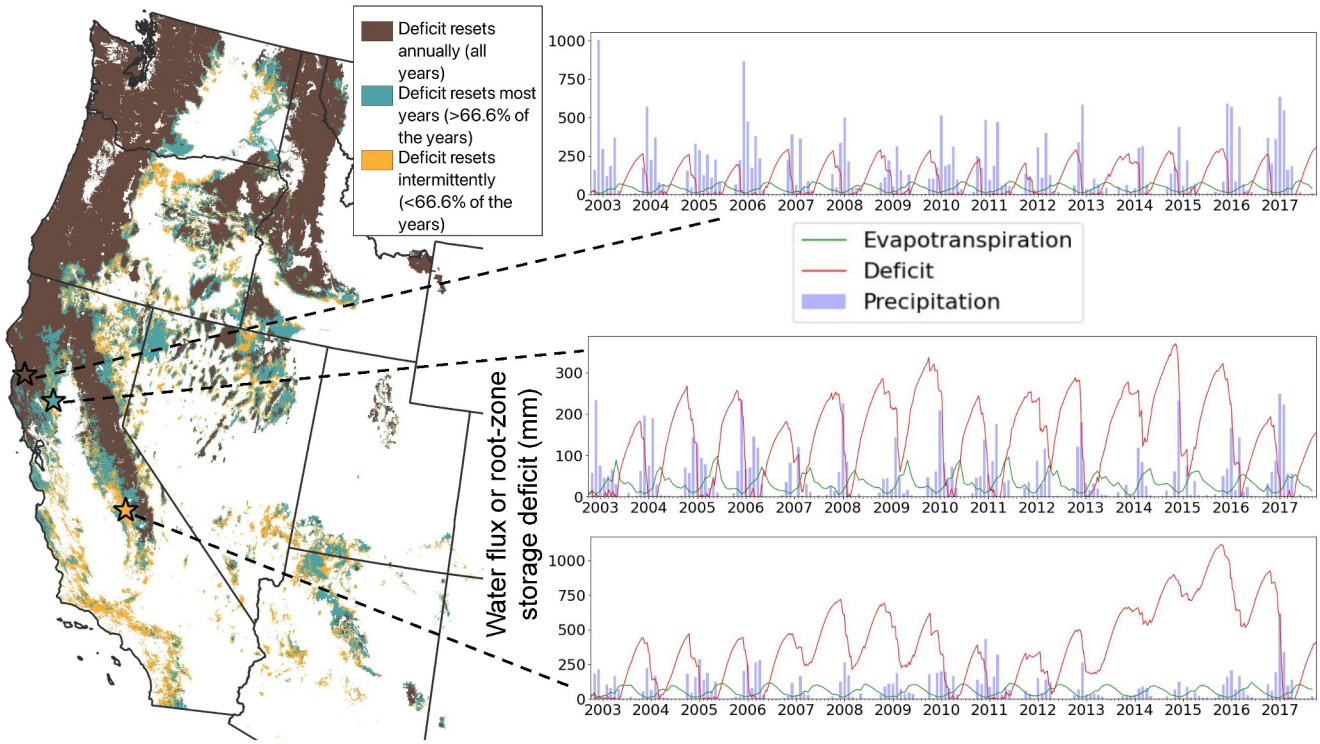

Figure 2. During the study period (1 October 2002–30 September 2017), the annual deficit returned to zero every year for the regions shown in brown (map on the left). Regions shown in teal and orange, respectively, did not reset in some years (<33% of the study period) or did not reset frequently, often for multiple years in a row (>33%). For each category, a corresponding example time series of the study period is shown on the right with the relevant fluxes necessary to compute root-zone storage deficit. In forests covering over 26,500 km^2 (land covers 1–5 in Figure S14 in Supporting Information S1), the root-zone storage deficit does not reset annually.

Geological Survey (USGS) National Land Cover Database (NLCD) land cover classification (L. Yang et al., 2018), and the Gridded National Soil Survey Geographic Database (Survey Staff, 2019). Excluding areas where depth to bedrock was greater than 1.5 m was due to the availability of soil water storage capacity estimates, which were limited to 1.5 m depth across CONUS. For a detailed description of the masking process see McCormick et al. (2021).

Gridded timeseries data used to inform the annual water balance was taken for the 2003–2017 water years (October 1–September 30). The same timeframe was analyzed using the multi-year deficit approach; however, the deficit was calculated from the start of the previous water year (1 October 2001) to account for the possibility that the deficit was not replenished at the beginning of the study period. In both cases, all data was analyzed using the Google Earth Engine Python application programming interface (API) (Gorelick et al., 2017). The study period was chosen to align with the availability of PML *ET* (Y. Zhang et al., 2019).

2.2. Evaluating Storage via Water Balances

Following McCormick et al. (2021), we estimate a lower-bound (minimum) on the maximum annual root-zone storage deficit (S_R) using the mass balance approached outlined by Wang-Erlandsson et al. (2016) and modified to account for snow cover by Dralle et al. (2021) (500 m pixel scale). The technique takes the running integrated difference of land-atmosphere water fluxes exiting (F_{out} [L/T] = *ET*) and entering (F_{in} [L/T] = P) at a pixel. *ET* is sourced from PML V2 (500 m pixel scale; Y. Zhang et al., 2019) to represent F_{out} and P (rain + snow meltwater equivalent; C. Daly, 2013) is extracted from PRISM (4,638.3 m pixel scale; C. Daly et al., 2015), to represent F_{in}. Input data was converted from native resolution (shown in parentheses above) to 1,000 m and re-projected to the World Geodetic System 1984 (EPGS:4326) for analysis.

First, the accumulated difference between F_{out} and F_{in} is taken for timeframe t_n to t_{n+1} and corrected for the presence of snow based on a snow cover threshold:

19447973, 2024, 8, Downloaded from https://agupubs.onlinelibrary.wiley.com/doi/10.1029/2023WR036719, Wiley Online Library on [21/08/2024]. See the Terms and Conditions (https://onlinelibrary.wiley.com/terms-and-conditions) on Wiley Online Library for rules of use; OA articles are governed by the applicable Creative Commons License

19447973, 2024, 8, Downloaded from https://agupubs.onlinelibrary.wiley.com/doi/10.1029/2023WR036719, Wiley Online Library on [21/08/2024]. See the Terms and Conditions (https://onlinelibrary.wiley.com/terms-and-conditions) on Wiley Online Library for rules of use; OA articles are governed by the applicable Creative Commons License

$$A_{t_n \to t_{n+1}} = \int_{t_n}^{t_{n+1}} (1 - \lceil C - C_0 \rceil) \cdot F_{out} - F_{in} \mathrm{d}t \quad (1)$$

where C_0 is a pre-defined threshold percentage of snow cover, C is snow cover, and $\lceil \cdot \rceil$ is the ceiling operator (rounds up to the nearest integer). When snow cover exceeds the threshold (i.e., $C > C_0$), the expression $(1 - \lceil C - C_0 \rceil)$ returns 0, ignoring ET when snow is present by setting $F_{out} = 0$; when $C \leq C_0$, $(1 - \lceil C - C_0 \rceil)$ returns 1 and F_{out} remains unaltered. This effectively avoids erroneously accumulating a storage deficit from ET during snowmelt when water may be infiltrating into the root zone (without the need to run a full snowmelt model). We use the Normalized Difference Snow Index (NDSI) snow cover band (Hall et al., 2016) to compute snow cover and set the snow cover threshold to 10%.

Second, the instantaneous root-zone storage deficit can be determined iteratively via the following equation:

$$D_{t_{n+1}} = \max(0, D_{t_n} + A_{t_n \to t_{n+1}}) \quad (2)$$

where $D_{t_{n+1}}$ is the deficit at time t_{n+1}. If the deficit falls below zero, the cumulative volume resets to zero as the subsurface has been replenished with water.

At each pixel, we compute the annual maximum observed deficit ($D_{\max}$, evaluated October 1 → September 30) and infer it to be a lower-bound on annual root-zone storage deficit ($S_R = D_{\max}$). Crucially, this assumes the root-zone storage deficit is replenished on a year-to-year basis which, in many parts of western US, has been shown to not be the case (e.g., Figure 2; Cui et al., 2022; Goulden & Bales, 2019; Hahm et al., 2022). We then separately calculate the root-zone storage deficit over the entire study period without enforcing annual replenishment to investigate multi-year deficit accrual using the non-resetting deficit model outlined in Section 2.3. We use Equation 2 to calculate D and track ET in excess of S_{soil} to infer the amount of evapotranspiration sourced from bedrock between 1 October 2002 (start) and 30 September 2017 (end):

$$S_{\substack{\max \\ t_{start} \to t_{end}}} = \max(D_{t_{start}}, D_{t_{start+1}}, \ldots, D_{t_{end}}) \quad (3)$$

$S_{bedrock(a)}$, the minimum annual amount of evapotranspiration sourced from bedrock water storage when resetting the deficit annually, is inferred to be the difference between the median (across years) annual maximum root-zone storage deficit and the soil water storage capacity reported by the Gridded National Soil Survey Geographic Database (Survey Staff, 2019). If the mean annual maximum root-zone storage deficit does not exceed the reported value by gNATSGO, we take this to mean that $S_{bedrock(a)}$ is not needed to explain annual evapotranspiration and set $S_{bedrock(a)} = 0$. This does not necessarily mean that bedrock water storage was not used to support evapotranspiration, but rather that this deficit tracking approach is unable to detect it.

2.3. Accounting for Multi-Year Deficit Accrual

The non-resetting deficit model represents an alternative approach to calculating $S_{bedrock}$, and is employed here as a means of corroborating the annually resetting mass balance inferences described above as well as account for regions where multi-year deficit accrual has been shown to occur (see Figure 2). Hereafter, all methods and results will be presented using the multi-year deficit approach and will follow the nomenclature $S_{bedrock(my)}$ to differentiate from the original, annually resetting water balance model ($S_{bedrock(a)}$). As above, the approach tracks the incoming and outgoing fluxes in excess of soil capacity to infer bedrock storage dynamics. However, the method presented below differs from the original water balance method in that it does not assume the deficit is reset annually, allowing for larger D values when $ET > P$ for extended periods (e.g., drought). To do so, the model prioritizes S_{soil} use during plant transpiration and prioritizes refilling S_{soil} when $P > ET$ and S_{soil} has not been fully replenished. S_{soil} and $S_{bedrock}$ can be used simultaneously (e.g., Cai et al., 2023; Rose et al., 2003), however, our model assumes only S_{soil} can be used when both are present. Because we have instructed the model to explicitly refill and deplete S_{soil} prior to bedrock use, the results also produce a lower-bound (conservative) estimate to $S_{bedrock(my)}$, as before.

19447973, 2024, 8, Downloaded from https://agupubs.onlinelibrary.wiley.com/doi/10.1029/2023WR036719, Wiley Online Library on [21/08/2024]. See the Terms and Conditions (https://onlinelibrary.wiley.com/terms-and-conditions) on Wiley Online Library for rules of use; OA articles are governed by the applicable Creative Commons License

First, we iteratively calculate the quantity of storage at each timestep during the study period:

$$S_{t_n \to t_{n+1}} = S_{t_n} + (P_{t_{n+1}} - ET_{t_{i+1}}) \tag{4}$$

where S is the running storage and $P_{t_{n+1}}$ and $ET_{t_{n+1}}$ are the total precipitation and evapotranspiration between timesteps t_n and t_{n+1}, respectively. Soil storage is assumed to be full at the beginning of the study period and, therefore, S is set to S_{soil} at t_n.

To calculate $S_{bedrock(my)}$, running soil storage must be constrained by soil storage capacity:

$$\begin{aligned} S_{t_{n+1}} &= 0 \quad if S_{t_{n+1}} < 0 \\ S_{t_{n+1}} &= S_{soil} \quad if S_{t_{n+1}} > S_{soil} \end{aligned} \tag{5}$$

where S_{soil} is the maximum amount of plant-available water capable of being stored in the soil profile. The lower-bound limit to storage is set at zero as storage cannot, by definition, be negative.

The total evapotranspiration inferred to be sourced from bedrock from time t_n to t_{n+1} is then calculated by taking the total ET in excess of soil storage:

$$\begin{aligned} S_{bedrock(my)_{t_{n+1}}} &= 0 \quad if ET_{t_{n+1}} - S_{t_{n+1}} < 0 \\ S_{bedrock(my)_{t_{n+1}}} &= ET_{t_{n+1}} - S_{t_{n+1}} \quad if ET_{t_{n+1}} - S_{t_{n+1}} > 0 \end{aligned} \tag{6}$$

Under these conditions, evapotranspiration sourced from bedrock can only occur once S_{soil} is fully depleted and assumes that all incoming inputs (i.e. P) are used to replenish S_{soil} before $S_{bedrock(my)}$. In other words, plant transpiration is assumed to prioritize the use of S_{soil} over $S_{bedrock(my)}$ and subsurface storage dynamics prioritize refilling S_{soil} prior to $S_{bedrock(my)}$. By retaining the difference between ET and S, the equation effectively accounts for the edge case scenario where only a portion of ET is sourced from bedrock during the timestep. For comparison to the original water balance method, the results are provided at an annual scale by taking the median value of the summed $S_{bedrock(my)}$ for each water year.

We additionally report the distribution of pixels that have observed multi-year deficit accruals during the study period to investigate the influence of extended drought conditions on water partitioning. Between 1 October 2002 and 30 September 2017, we calculate the number of years where the deficit was not replenished by taking the minimum root-zone storage deficit ($D_{\min}$) observed each water year for all pixels. If $D_{\min} > 0$ in a given water year, we take that to mean that the deficit was not replenished in that water year. The resulting pixels were divided into three classes: (a) Deficit resets annually (all years), (b) Deficit resets most years (>66.6% of the years), and (c) Deficit resets intermittently (<66.6% of the years) (Figure 2).

In the following sections, we outline the processes used to investigate the role of $S_{bedrock(my)}$ on water partitioning, latent heat fluxes, and dry-season plant transpiration timing. In each case, the methods are informed using the modified water balance that accounts for non-resetting deficits and, thus, provides a more accurate estimation of bedrock water use.

2.4. Water Partitioning and Timing

Within the Budyko (1974) framework, the long-term partitioning of P into ET and Q is a function of the long-term ratio of PET to P. Under these conditions, Q is assumed to include both overland flows and lateral subsurface flows resulting from infiltration, and storage changes are assumed to be negligible ($\Delta S \approx 0$). We took observed evaporative indices ($\epsilon_{obs} = ET/P$) by dividing the median annual evapotranspiration by precipitation for the 2003–2017 water years using data collected from the gridded products described above. We also infer what the evaporative index would be if plants did not have access to bedrock water ($\epsilon_{w/o\ bedrock}$) by removing $S_{bedrock(my)}$ (the minimum amount of bedrock water used in year when accounting for multi-year deficit accrual) from the observed evaporative index. If S_R does not exceed S_{soil}, then our method cannot detect the influence of bedrock on the evaporative index:

$$\epsilon_{w/o\ bedrock}\begin{cases} ET_{obs} / P & \text{if } S_R \le S_{soil} \\ (ET_{obs} - S_{bedrock(my)}) / P & \text{if } S_R > S_{soil} \end{cases} \quad (7)$$

Following this, the relative change (expressed as a percentage) in evaporative index without access to bedrock water is the difference between $\epsilon_{w/o\ bedrock}$ and ϵ_{obs} relative to ϵ_{obs}:

$$\Delta\epsilon = \left(\frac{\epsilon_{w/o\ bedrock} - \epsilon_{obs}}{\epsilon_{obs}}\right) * 100 \quad (8)$$

Streamflow data from 128 minimally impacted USGS watershed gauges in the western US are in agreement (Nash-Sutcliffe efficiency of 0.93) with the precipitation (PRISM) and evapotranspiration (PML) data used in our analysis (Figure S2 in Supporting Information S1). Therefore, we find it reasonable to estimate Q from the water balance (i.e., $Q = P - ET$). Because our analysis is performed at the pixel rather than catchment scale, there is potentially a greater risk of difficult-to-quantify net inter-pixel groundwater flow. However, the pixel scale in this study is generally greater than the scale of individual hillslope-channel units, where lateral groundwater flows could be expected to be most relevant. Furthermore, because pixels with depths to bedrock >1.5 m were masked from the analysis, convergent valley bottoms where net import of groundwater may be likely to occur tend to be excluded from our analysis. We calculated the runoff ratio (RR) as the difference between one and the observed evaporative index ($RR = 1 - \epsilon$).

Finally, we compute the median first month of year ($MOY_{bedrock}$) when bedrock must be used to explain observed evapotranspiration, by determining the observed month (for the 2003–2017 water years) when $S_{bedrock(my)}$ is first used based on the methods outlined in Section 2.3, implying any evapotranspiration sourced from the subsurface from the start of the deficit accrual to beyond this date must include water sourced from bedrock storage. This does not mean that bedrock storage was not accessed in prior months but rather that it cannot be tracked using the deficit approach. As such, $MOY_{bedrock}$ represents the latest possible month that plants must be using, or have already used, bedrock water to sustain plant transpiration.

2.5. Energy Partitioning

In the following section, we infer the monthly total latent heat flux associated with evapotranspiration sourced from bedrock. The latent heat, that is, the energy required to change from the liquid to vapor phase, is equal to the energy required to evaporate the accrued monthly deficit (in mm of water) beyond that provided by soil. We report this value in units of power per unit of area (W/m^2).

First, following the processes outlined in Section 2.3, the total evapotranspiration inferred to be sourced from bedrock water storage between 2 months is computed using Equations 4–6 where t_n and t_{n+1} are the first day of the target month and following month, respectively. Because the period of coverage for ET (PML V2) is 8 days, $S_{bedrock\ (my)}$ must be adjusted to account for the missing coverage at the beginning and/or end of each month (i.e., when the acquisition dates do not fall on the first of each month). If this is the case, ET is converted to daily scale (i.e. divided by 8) and only the proportion of ET that occurred during the target month is counted by multiplying the daily value by the number of days in the target month. This method assumes ET is constant during the 8-day return period.

The above calculation assumes that plants first exhaust any available soil water and subsequently use bedrock water. If plants exhaust soil water and bedrock water simultaneously throughout the dry season, the method used here to quantify the total latent heat flux associated with bedrock water during the dry season is not erroneous but rather would shift the bedrock-associated latent heat flux patterns earlier into the dry season.

Second, $S_{bedrock(my),month}$ (mm) is converted to power per unit area metric (E_e) based on the enthalpy of vaporization of a known mass of water:

$$E_e = (S_{bedrock(my),month}) * (\rho_w) * (\Delta H_v) * (1/t) \quad (9)$$

where ρ_w is the density of water (1,000 g/L), ΔH_v is the latent heat of vaporization of water (2,257 J/g), which we do not adjust for local variations in temperature or pressure, and t is the total seconds between the ith and $i + 1$st

19447973, 2024, 8, Downloaded from https://agupubs.onlinelibrary.wiley.com/doi/10.1029/2023WR036719, Wiley Online Library on [21/08/2024]. See the Terms and Conditions (https://onlinelibrary.wiley.com/terms-and-conditions) on Wiley Online Library for rules of use; OA articles are governed by the applicable Creative Commons License

19447973, 2024, 8, Downloaded from https://agupubs.onlinelibrary.wiley.com/doi/10.1029/2023WR036719, Wiley Online Library on [21/08/2024]. See the Terms and Conditions (https://onlinelibrary.wiley.com/terms-and-conditions) on Wiley Online Library for rules of use; OA articles are governed by the applicable Creative Commons License

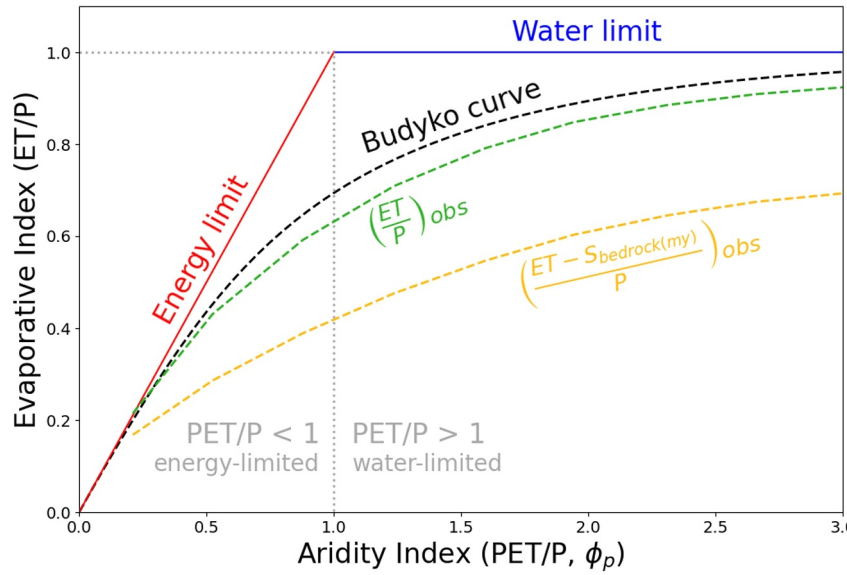

Figure 3. The Budyko (1974) plotting space with the Budyko curve (dashed black line), that is, $\frac{ET}{P} = \left\{\phi_p \tanh\left(\frac{1}{\phi_p}\right)\left[1 - \exp\left(-\phi_p\right)\right]\right\}^{\frac{1}{2}}$, compared to observed *ET*/*P* versus *PET*/*P* (green) and observed $ET - S_{bedrock(my)}$/P versus *PET*/*P* (orange) during the study period (2003–2017 water years) in western CONUS. Observed *ET*/*P* is binned every 4% (i.e., 25 bins) based on the median value and smoothed using the Savitzky-Golay filter function (available in scipy.signal library). Theoretical water and energy limits are shown in blue and red. Removing evapotranspiration inferred to be a result of access to $S_{bedrock(my)}$ dramatically lowers the curve.

month (1 mm of liquid water per square meter is 1 L). The resulting value is a median latent heat flux per second (i.e. power, W) per m^2 (unit area) for a given time frame.

3. Results

Our primary findings are that (a) soil water storage capacity (S_{soil}) does not explain deviations from the Budyko-curve in asynchronous climates (Figure S4 in Supporting Information S1), (b) the proportion of terrestrial precipitation returned to the atmosphere (vs. streamflow) is strongly influenced by plant use of bedrock water reserves (Figure 4), (c) subsurface storage deficits are not always fully replenished in a given year (Figure 2), (d) $S_{bedrock}$ is needed to sustain dry season plant transpiration early into the growing season (Figure 5), and (e) the summer latent heat flux associated with evapotranspiration of bedrock water is substantial (Figure 7) and warrants further research with respect to land surface energy interactions. Below, we expand on these findings and highlight particular regions of interest where $S_{bedrock}$ plays an important role in the local water and energy partitioning patterns.

3.1. Deviations From the Budyko-Curve Are Poorly Explained by Soil Water Storage Capacity

Across the asynchronous climate ($ASI \geq 0.40$) study area, the aridity index explains the primary trend in the evaporative index for individual pixels, consistent with the Budyko (1974) findings for catchments (Figure 3). However, for a given aridity index, there remain deviations from the curve. It is a commonly hypothesized that, for a particular climate (here, in addition to controlling for *PET*/*P* also controlling for seasonality by virtue of the large *ASI*), subsurface storage deficit may explain deviations from the Budyko-curve (Miller et al., 2012). Using the catchment characteristic n to quantify differences in the evaporative index for a particular aridity index (H. Yang et al., 2008), where higher n denotes higher *ET*/*P* for a given aridity index, we find that soil water storage capacity (S_{soil}) alone does not explain ($R^2 = -0.01$) the variance in n and, therefore, is a poor explanation for deviations from the Budyko-curve across western US (Figure S4 in Supporting Information S1 inset). Indeed, S_{soil} accounts for only a portion of the below-ground storage capacity and, in many places, is comparatively small relative to $S_{bedrock}$ (e.g., McCormick et al., 2021). Moreover, removing *ET* sourced from bedrock ($S_{bedrock(my)}$)

10.1029/2023WR036719

19447973, 2024, 8, Downloaded from https://agupubs.onlinelibrary.wiley.com/doi/10.1029/2023WR036719, Wiley Online Library on [21/08/2024]. See the Terms and Conditions (https://onlinelibrary.wiley.com/terms-and-conditions) on Wiley Online Library for rules of use; OA articles are governed by the applicable Creative Commons License

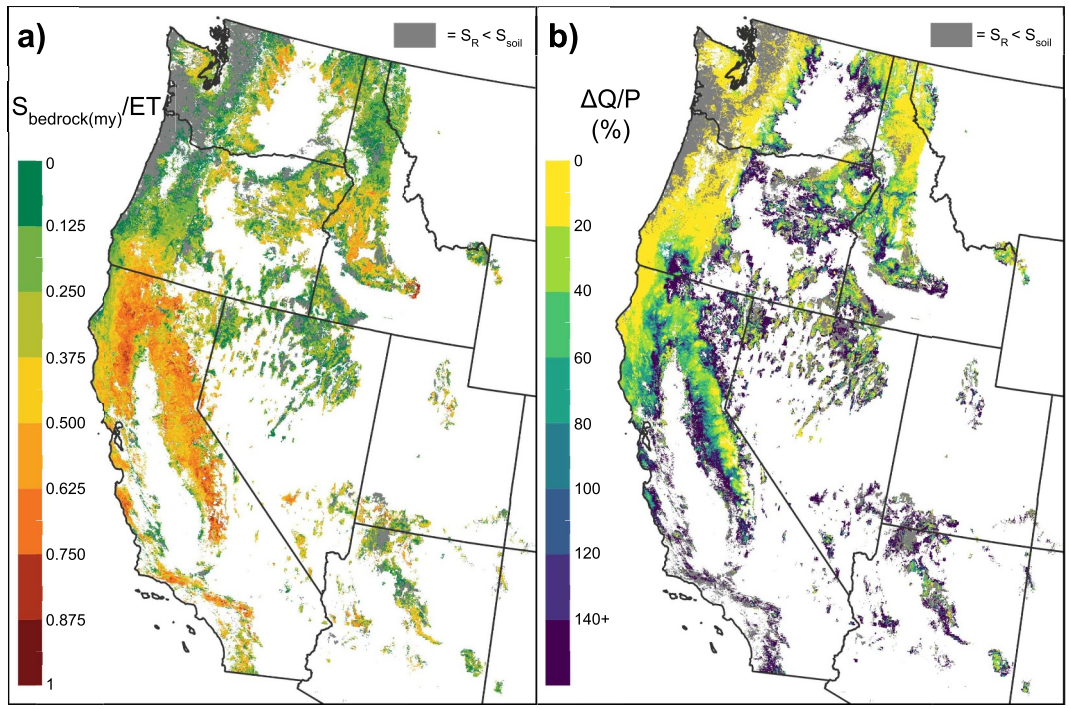

Figure 4. (a) Median annual evapotranspiration inferred to be sourced from bedrock water relative to annual evapotranspiration when accounting for multi-year deficit accrual. (b) The relative change in runoff ratio when evapotranspiration inferred to be sourced from bedrock storage ($S_{bedrock(my)}$) is removed, that is, $(ET - S_{bedrock(my)})/P$. (a) Inspired by Figure 3 of McCormick et al. (2021). Across large areas of the western US, annual evapotranspiration would be hundreds of millimeters less and the proportion of precipitation returned to the streams would increase without access to bedrock water.

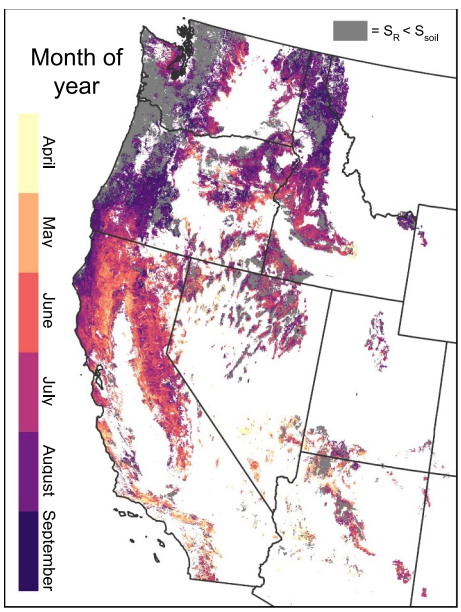

Figure 5. Typical month in which the annual root-zone storage deficit (S_R) exceeds the soil water storage capacity (S_{soil}), implying plant transpiration beyond this point must be using $S_{bedrock(my)}$ to sustain transpiration and growth. Bedrock water is accessed very early into the growing season for many parts of the western US.

drastically shifts the Budyko-curve downwards (Figure 3), further highlighting the importance of including both S_{soil} and $S_{bedrock}$ in the context of hydrologic partitioning.

3.2. Large Proportions of the Precipitation Returned to the Atmosphere Is Sourced From $S_{bedrock}$

In the following section, the spatial patterns of $S_{bedrock}$, ET/P, and Q/P in the western US, derived using the annual ($S_{bedrock(a)}$) and multi-year ($S_{bedrock(my)}$) water balance methods, are presented. Figure 4 shows the spatial patterns of evapotranspiration inferred to be sourced from bedrock and relative change in runoff ratio without access to bedrock ($\Delta Q/P$) using the multi-year water balance method (see Figure S9 in Supporting Information S1 for derivation). In each case, areas shown in gray represent pixels where bedrock-derived ET was unable to be identified by the proposed methods.

Broadly, both evapotranspiration inferred to be sourced from bedrock ($S_{bedrock(my)}$) and relative runoff ratio without access to bedrock water ($\Delta Q/P$) increases southward from the USA-Canada border (Figure 4). The opposite is true for relative evaporative index ($\Delta ET/P$), which decreases southward toward the USA-Mexico border (Figure S6 in Supporting Information S1). In particular, the Northern California Coast Ranges, the southern Cascades, the Transverse Ranges and the Sierra Nevada are most reliant on $S_{bedrock(my)}$ for dry season plant transpiration. The median change in relative runoff ratio (evaporative index) of all pixels in the western US that detected $S_{bedrock(my)}$ use was +26.0 (−25.9)% using the

19447973, 2024, 8, Downloaded from https://agupubs.onlinelibrary.wiley.com/doi/10.1029/2023WR036719, Wiley Online Library on [21/08/2024]. See the Terms and Conditions (https://onlinelibrary.wiley.com/terms-and-conditions) on Wiley Online Library for rules of use; OA articles are governed by the applicable Creative Commons License

multi-year deficit method (Figure 4, Figures S8 and S9 in Supporting Information S1). That is to say, access to bedrock water results in a greater partitioning of P to ET and less to Q. Up to 1,072 mm of evapotranspiration is inferred to be sourced from bedrock water with a median value of 93.7 mm across all pixels (Figure 4). Evapotranspiration sourced from bedrock using the deficit approach (i.e., $S_R < S_{soil}$) could not be detected in areas highlighted in gray. These areas are mostly limited to the coastal Pacific Northwest, where the aridity index tends to be lower than the rest of the region (Figure S3 in Supporting Information S1), and account for roughly one quarter of all pixels in the study.

The annual water balance model driven by a resetting deficit makes qualitatively similar estimates to the multi-year deficit approach. However, the annual approach drastically underestimates the contribution of $S_{bedrock}$ in areas that do not reset annually (Figures S5 and S11 in Supporting Information S1). The median difference between $S_{bedrock(my)}$ and $S_{bedrock(a)}$ was 41.8 mm and, in some cases, several hundred millimeters of bedrock storage was not accounted for using the annual water balance. For a more detailed view of the spatial distribution of $S_{bedrock(a)}$, including full CONUS coverage, see McCormick et al. (2021). The median change in relative runoff ratio (evaporative index) of all pixels in the western US that detected $S_{bedrock(a)}$ use was +15.4 (−13.5)% using the annual water balance (Figures S6 and S7 in Supporting Information S1). That is to say, access to bedrock water reserves favors ET over Q. Up to 782 mm of evapotranspiration is inferred to be sourced from bedrock water with a median values of 49.0 mm across all pixels (Figure S5 in Supporting Information S1).

The percentage of pixels where the deficit was determined to reset most years (>66.6%) and infrequently (<66%) was 22.9% and 15.4%, respectively (Figure 2). In all categories, the proportion of ET inferred to be sourced from bedrock storage was greater using the multi-year deficit approach compared to the annual approach (Figure 6, Figure S10 in Supporting Information S1). The median proportion of ET inferred to be sourced from bedrock increased from 10.8% to 20.6%, 14.9% to 30.6%, and 18.3% to 35.9% when accounting for a multi-year deficit in regions where the deficit reset annually (all years), frequently (>66% of the years), and intermittently (<66.6%), respectively. Even in regions where the deficit does reset annually, the proportion of ET sourced from bedrock is underestimated using the annual water balance because it assumes S_{soil} is fully replenished by October 1 and that $P > ET$ over every timestep of the wet season, both of which are rarely the case.

3.3. $S_{bedrock}$ Is Needed to Sustain Plant Transpiration Early Into the Growing Season and Contributes Substantial Latent Heat Flux as Summer Progresses

Regions of high $S_{bedrock(my)}$ (Figure 4) also correspond to areas that require $S_{bedrock(my)}$ to sustain plant transpiration early into the growing season (Figure 5, Figure S13 in Supporting Information S1) and involve large bedrock-water associated latent heat fluxes in the hot summer months (Figure 7). The median first day of the year when $S_{bedrock(my)}$ is needed to account for evapotranspiration is 209 (July 28) and 24.4% of the study area must use bedrock water to account for ET prior to the beginning of summer (June 21) (Figure S12 in Supporting Information S1). As early as June, large portions of western CONUS have a noticeable latent heat flux associated with ET sourced from bedrock. Across the entire study area, the median latent heat flux is 0.510, 4.51, 14.3, 23.3, and 18.6 W/m^2 from May to September (Figure 7). After removing regions where bedrock is not needed to account for ET (i.e., gray in Figures 4 and 5), the median latent heat fluxes increase to 1.71, 9.32, 22.9, 35.6, and 27.0 W/m^2, respectively. In some parts of California, there are upwards of 200 W/m^2 associated with bedrock-derived ET throughout the summer.

4. Discussion

The findings presented in this study highlight the importance of $S_{bedrock}$ on water and energy partitioning in the western US. Below we discuss the possible implications of these findings on land-atmosphere interactions. We begin by situating our study within the context of the Budyko framework and discuss how this influences hydrologic partitioning. We then discuss the role of factors like geology on controlling the amount of $S_{bedrock}$ and, consequently, hydrologic, energy, and nutrient partitioning. Finally, we address limitations to our study and offer potential future opportunities to advance the topic.

4.1. $S_{bedrock}$ Controls on Water and Energy Partitioning

The catchment water balance in asynchronous climates often deviates substantially from expectations set by the Budyko curve (Berghuijs et al., 2020; De Lavenne & Andréassian, 2018; Potter et al., 2005; Viola et al., 2017).

19447973, 2024, 8, Downloaded from https://agupubs.onlinelibrary.wiley.com/doi/10.1029/2023WR036719, Wiley Online Library on [21/08/2024]. See the Terms and Conditions (https://onlinelibrary.wiley.com/terms-and-conditions) on Wiley Online Library for rules of use; OA articles are governed by the applicable Creative Commons License

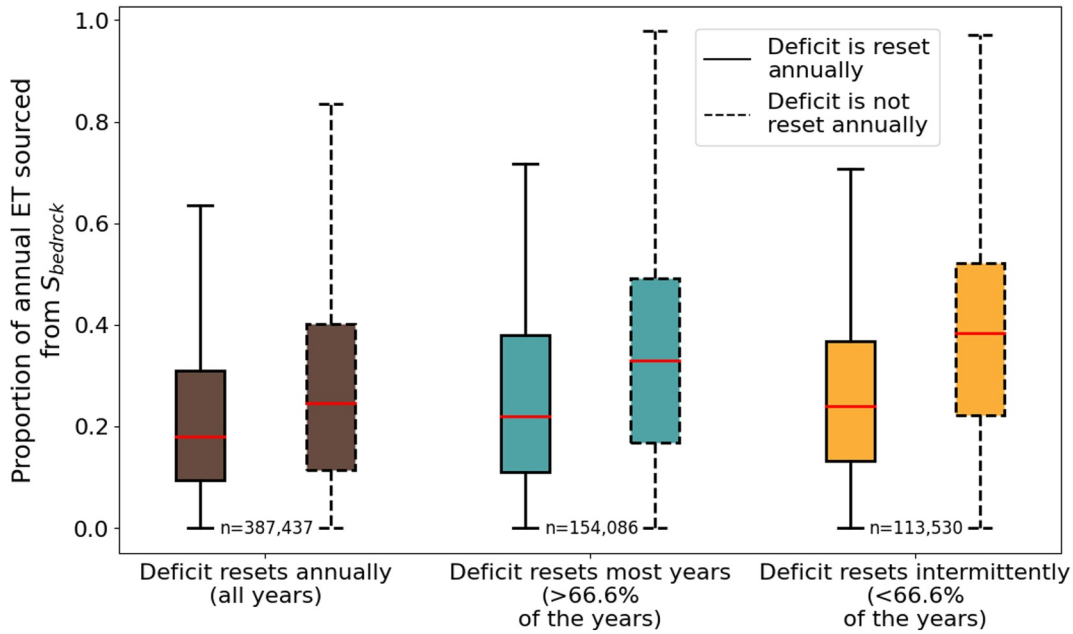

Figure 6. The proportion of annual evapotranspiration that is sourced from $S_{bedrock}$ when the deficit is reset annually ($S_{bedrock(a)}$) versus not reset annually ($S_{bedrock(my)}$). Boxplots are grouped based on the three classes outlined in Section 2.3 and match the color of the pixels in Figure 2. Two-sample Kolmogorov-Smirnov (K-S) tests yielded p-values < 0.0001 for each classification. The number of pixels for each class is found between each boxplot pairing. Pixels that did not detect bedrock-derived *ET* were excluded from the plot. The water balance method informed by an annual resetting deficit underestimates $S_{bedrock}$ contribution in asynchronous climates.

Previous studies have shown the importance of seasonality (Feng et al., 2012; Gerrits et al., 2009; Hickel & Zhang, 2006; Xing et al., 2018; Yokoo et al., 2008) and water storage capacity (Chen et al., 2013; Cheng et al., 2022; E. Daly et al., 2019; Donohue et al., 2012; Gentine et al., 2012; Hahm et al., 2019; Hickel & Zhang, 2006; Milly, 1994a, 1994b; Potter et al., 2005; Rodriguez-Iturbe et al., 1999; Williams et al., 2012; Woods, 2003) within the context of the Budyko framework and many have highlighted that *ET* is favored with increasing soil water storage capacity (Feng et al., 2012; Milly, 1994a, 1994b; Padrón et al., 2017; Porporato et al., 2004). We take this analysis a step further, by differentiating soil from bedrock, to elucidate basic features of how root-zone water is divided between hydrogeologically distinct subsurface layers. Our results suggest S_{soil} alone poorly explains deviations from the Budyko-curve (Figure S4 in Supporting Information S1), and indicate that $S_{bedrock}$ plays a comparatively larger role on controlling hydrologic partitioning in the western US. This is confirmed by our findings in Figure 4 and is in agreement with similar findings by McCormick et al. (2021), and hillslope-scale observational studies (Dralle et al., 2018; Hahm et al., 2019, 2022; Lapides, Hahm, Rempe, Dietrich, & Dralle, 2022; Rempe & Dietrich, 2018). Moreover, if $S_{bedrock}$ influences near-surface climate properties in a similar manner to soil moisture (e.g., Brabson et al., 2005; Haarsma et al., 2009; Koster et al., 2004), current GCMs may under-estimate the influence of subsurface storage on extreme temperatures and heat waves (e.g., Diffenbaugh et al., 2007; Seneviratne et al., 2006), precipitation formation (e.g., Alfieri et al., 2008; Ek & Holtslag, 2004; Taylor, 2015), and changes in planetary boundary layer (PBL) circulation patterns (e.g., Ookouchi et al., 1984; Sousa et al., 2020). In particular, we highlight the large latent heat flux patterns associated with bedrock-derived *ET* in California, which is rarely accounted for in GCMs, and emphasize the need for integration of $S_{bedrock}$ into climate and vegetation models in seasonally dry climates (e.g., Lapides et al., 2024).

4.2. $S_{bedrock}$ Influences on Runoff Generation

Some forms of runoff generation require unsaturated storage deficits to be replenished prior to significant runoff production (McDonnell et al., 2021; Sayama et al., 2011). Recently, Lapides, Hahm, Rempe, Whiting, and Dralle (2022) showed that the "missing" snowmelt runoff during the 2021 spring melt period in California (California Department of Water Resources, 2021) could be attributed to deep root-zone storage deficits caused

10.1029/2023WR036719

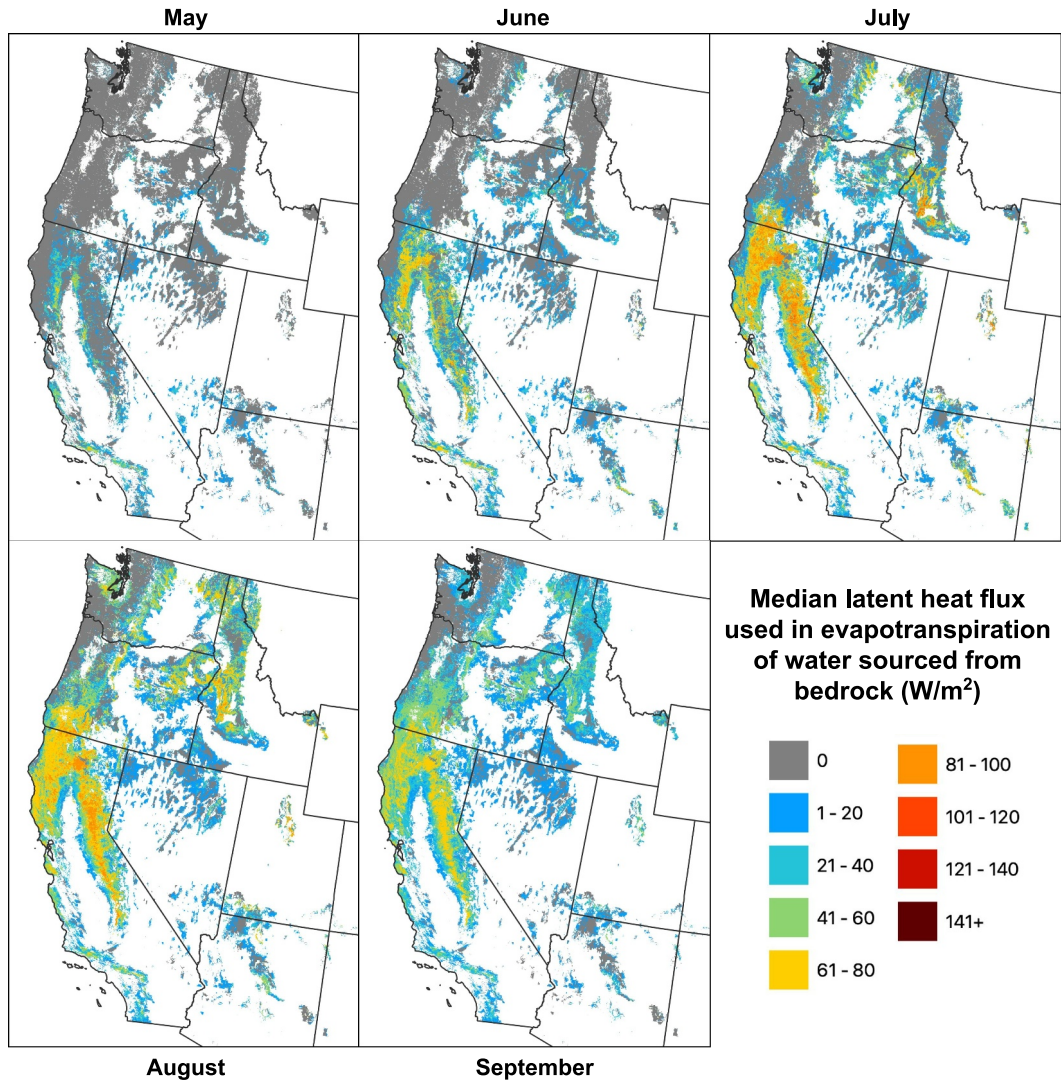

Figure 7. Median latent heat flux (equivalent units to solar irradiance, W/m^2) used in evapotranspiration that is sourced from $S_{bedrock}$ during the growing season. In large parts of the western US, in particular northern California and the Sierra Nevada mountain ranges, a large latent heat flux is associated with evapotranspiration of bedrock water every summer.

by drought conditions. These areas, and many other parts of the western US, have among the largest observed S_R in the contiguous US and the fraction of S_R attributed to bedrock is substantial (McCormick et al., 2021). Our results agree with these findings and highlight that $S_{bedrock}$ has major implications for runoff generation in the mountainous West. Deficit-based approaches represent a potential method for scaling up hillslope (e.g., S. P. Anderson et al., 1997; Salve et al., 2012; Tromp-van Meerveld et al., 2007) and catchment (e.g., Ajami et al., 2011; Sayama et al., 2011) studies to explain and predict runoff production—the "Holy Grail" of hydrology (Beven, 2006)—at large scales. While our findings suggest bedrock storage heavily influences runoff patterns, especially in southwest of the study area (Figure 4), there is a need for more studies investigating these dynamics and, in particular, field-scale studies to confirm the trends presented here.

4.3. Geological Influences on $S_{bedrock}$ as a Controlling Factor in Vegetation Structure

Evidence supporting the notion that forest ecosystems rely on moisture stored in weathered bedrock to sustain dry season growth goes back several decades (e.g., Arkley, 1981; Jones & Graham, 1993). In many cases, bedrock water constitutes a majority of the total subsurface water available to sustain plant transpiration (e.g., M. A. Anderson et al., 1995; McCormick et al., 2021; Rose et al., 2003). Here, we demonstrate that bedrock

19447973, 2024, 8, Downloaded from https://agupubs.onlinelibrary.wiley.com/doi/10.1029/2023WR036719, Wiley Online Library on [21/08/2024]. See the Terms and Conditions (https://onlinelibrary.wiley.com/terms-and-conditions) on Wiley Online Library for rules of use; OA articles are governed by the applicable Creative Commons License

19447973, 2024, 8, Downloaded from https://agupubs.onlinelibrary.wiley.com/doi/10.1029/2023WR036719, Wiley Online Library on [21/08/2024]. See the Terms and Conditions (https://onlinelibrary.wiley.com/terms-and-conditions) on Wiley Online Library for rules of use; OA articles are governed by the applicable Creative Commons License

storage dynamics influence water and energy partitioning at large scales and throughout many parts of the western US. It is, therefore, necessary to discuss the controlling factors on bedrock formation and structure as these properties dictate the quantity of plant-available water held in fresh and weathered bedrock. The extent of bedrock weathering impacts pore size distribution with depth, and therefore plant-available water storage properties (Dawson et al., 2020; Klos et al., 2018). These properties in turn depend on climate, tectonics, and geology (Riebe et al., 2017). The mechanisms responsible for the transformation of fresh to weathered bedrock, which in turn increases subsurface moisture storage potential, are well established (see for overview, e.g., Brantley, 2010; Graham et al., 2010) but remain difficult to investigate due to limitations in accessing deep bedrock samples (see for overview, e.g., Zanner & Graham, 2005). Recently, studies have begun investigating the role of geology as a bottom-up control on root-zone storage capacity. One example of a study using deep bedrock samples found that root-zone storage deficits and plant community composition differed drastically in two adjacent, climatically similar watersheds in California due to contrasting geological substrates (Hahm et al., 2019). In another study, Hahm et al. (2024) used water fluxes to highlight areas where geologic substrates overlapped with lower than "climatically expected" S_R and argued that plant transpiration in these areas is inhibited directly by porosity and/or permeability (e.g., Hahm et al., 2019; Jiang et al., 2020; H. Liu et al., 2021) or indirectly via nutrient limitation (e.g., Hahm et al., 2014) and toxicity (e.g., Kruckeberg, 1992). However, research in this area remains limited owing to the fact that weathered bedrock profiles are challenging to access and investigate.

4.4. The Role of $S_{bedrock}$ on Biogeochemical Cycling

Our findings that plant water use from bedrock impacts water partitioning has implications for biogeochemical cycling. The importance of soil respiration in the global carbon cycle is well-documented (Janssens et al., 2001; Schimel, 1995). However, it remains a challenge to quantify the extent to which carbon dioxide (CO_2) is produced below the near-surface soil mantle in weathered bedrock. In Northern California, weathered bedrock has been shown to produce a substantial amount of CO_2 by contributing to soil efflux and as an inorganic carbon flux to groundwater and stream water (Tune et al., 2020). Similar findings in France suggest bedrock-derived CO_2 production can rival soil respiration (Soulet et al., 2021). Moreover, rock respiration can lead to increased porosity and weathering (Kim et al., 2017; Winnick et al., 2017) and remains active during the dry season after soil water has been fully depleted (Tune et al., 2020). The role of bedrock on nutrient cycling is not limited to carbon. Bedrock is the largest terrestrial nitrogen reservoir on Earth (Johnson & Goldblatt, 2015) and, yet, most nitrogen cycle models do not account for bedrock-derived nitrogen. For example, forests have been shown to source a similar amount of nitrogen from weathered bedrock compared to atmospheric sources in the Klamath Mountains (Morford et al., 2016). Findings by Wan et al. (2021) suggest that between 10% and 20% of global terrestrial N-N_2O flux may be sourced from bedrock weathering. Many other nutrients, including those that are primarily derived from bedrock mineral weathering (e.g., phosphorus, calcium, magnesium, etc.), are essential to plant growth.

The vertical and lateral flow of water in the subsurface regulates chemical weathering and nutrient cycling (Brantley et al., 2017; Manning et al., 2013; Torres et al., 2015). Bedrock fractures and soil matrix have different hydrologic properties, resulting in preferential flow patterns that alter how water interacts with mineral surfaces (Nimmo, 2021; Salve et al., 2012). For example, the distribution of water expedites weathering in the form of ion transport (Buss et al., 2008), dissolution (Hasenmueller et al., 2017), biological weathering (Finlay et al., 2020; Pawlik et al., 2016), and more. Recently, the Critical Zone (CZ) sciences community has proposed methods for predicting weathered bedrock patterns (Riebe et al., 2017) based on advancements in geophysics (e.g., Slim et al., 2015; St. Clair et al., 2015), geochemistry (e.g., Brantley et al., 2013; Lebedeva & Brantley, 2013; Lebedeva et al., 2007), and geomorphology (e.g., R. S. Anderson et al., 2013; Rempe & Dietrich, 2014). A reliable and testable method for predicting weathered bedrock patterns could provide the additional context necessary to formulate and test hypotheses on the role of bedrock on nutrient and water cycling. It is often thought that, under an evolving climate, the distribution of vegetation is primarily controlled by climate variables. However, some research suggests that geologic factors may have a stronger impact on regional diversity and, therefore, prioritizing the protection of geophysical settings is more appropriate for long-term conservation of biodiversity (M. G. Anderson & Ferree, 2010). Although our findings primarily focus on the magnitude of bedrock water, we underscore the necessity to further investigate the link between and bedrock water and biogeochemical cycles as we move toward a holistic approach in CZ sciences.

19447973, 2024, 8, Downloaded from https://agupubs.onlinelibrary.wiley.com/doi/10.1029/2023WR036719, Wiley Online Library on [21/08/2024]. See the Terms and Conditions (https://onlinelibrary.wiley.com/terms-and-conditions) on Wiley Online Library for rules of use; OA articles are governed by the applicable Creative Commons License

5. Limitations

Throughout this paper, several assumptions have been made that require further discussion. First, the assumption that *ET* does not contribute to F_{out} when a pixel is snow covered is not a presumption of how *ET* would function during the winter but a conservative assumption in light of uncertainties regarding snowmelt dynamics. *ET* may be considerable when snow cover is present and during snowmelt periods (e.g., Cooper et al., 2020; Kelly & Goulden, 2016; Kraft & McNamara, 2022) but implementing a spatially and temporally resolved snowmelt model at this scale would be challenging. Not allowing for *ET* to occur during snowmelt periods results in an under-estimation of *ET* (Dralle et al., 2021) and would, therefore, result in smaller $S_{bedrock}$ values. Second, our analysis occurs at pixel scale but is placed in the context of the Budyko framework, which is traditionally applied at the catchment scale under steady-state conditions. Recently, the validity of assuming negligible long term storage change at catchment-scale has been challenged (e.g., Condon et al., 2020; Fan, 2019; Safeeq et al., 2021) and few, if any, studies have considered these implications at pixel scale. For the purpose of the above analysis, the masking process excludes topographically convergent pixels (i.e., valleys). Even at steady-state, inter-pixel flux movements may not be zero but, due to the pixel selection process, are likely to be net exporters of water. In other words, the assumption would result in a net loss of water in the root-zone over time and, thus, the reported values of S_R and $S_{bedrock}$ are minimum estimates. Our methods cannot determine whether water was sourced from the unsaturated or saturated zone and are unable to detect deep groundwater movement.

Basing our study on distributed, remotely sensed, or spatially interpolated data sets may introduce substantial uncertainty in the results. All remotely sensed data is inherently limited by systematic errors (e.g., cloud filtering, sensors, etc.) and relies on ground truth data to validate uncertainty. The deficit-based approach used to estimate S_R and, by extension $S_{bedrock}$, is reliant on the accuracy of the water flux data (i.e., P, *ET*) and, thus, warrants further discussion. Remotely sensed *ET* remains one of the most challenging water fluxes to accurately predict due to the complexity of the atmospheric and surface conditions that inform *ET* models. PML and other satellite-derived *ET* products tend to over-estimate *ET* during the dry season and under-estimate *ET* during the wet season (Awada et al., 2021; Ji et al., 2021). Nevertheless, we are comfortable using PML V2 as it is calibrated using a widely distributed network of 95 flux towers (Y. Zhang et al., 2019) and performs strongly when compared against other *ET* products (He et al., 2022; Tao et al., 2024). Many of the areas highlighted in this study include mountainous regions which are difficult to validate owing to the lack of distributed observation networks (Bales et al., 2006). PRISM has been shown to under-estimate precipitation in complex, high-elevation terrains (e.g., Henn et al., 2018; Kunkel et al., 2013; Lundquist & Cayan, 2007) which would result in higher estimates of S_R and $S_{bedrock}$. Indeed, C. Daly et al. (1994) recognized these limitations to PRISM in their original model formulations and have made efforts to adjust the physiographically sensitive PRISM interpolation process over time (C. Daly et al., 2008). Subsequent studies have shown strong agreement between PRISM grids and ground-truthed temperature (Strachan & Daly, 2017) and precipitation (C. Daly et al., 2017) data and, in our study area, we found that precipitation (PRISM) in excess of evapotranspiration (PML) aligned well with USGS streamflow data in 128 minimally impacted catchments (Figure S2 in Supporting Information S1 and Rempe et al., 2022).

Due to challenges in directly observing water storage dynamics and plant uptake in bedrock there are limited field data to validate our inferences; however, McCormick et al. (2021) synthesized existing data sets and found the observations that were consistent with deficit-based methods. Moreover, the selected time series representing the three classes of deficit replenishment (colored stars in Figure 2) were not chosen at random, but rather, are three field sites where extensive subsurface storage dynamics have been monitored (brown: Rempe & Dietrich, 2018, teal: Hahm et al., 2022, and orange: O'Geen et al., 2018). In each case, our findings align well with the in situ observations presented by the above studies. The accuracy of satellite-based data has improved dramatically in recent decades (Dubovik et al., 2021) and, when coupled with finer-scale field studies (i.e., watershed to hill-slope), allows for regional study of topics that underpin important hydrologic problems. While we are confident in the data presented here we emphasize the need to further implement field-based studies.

An additional source of uncertainty lies in using gNATSGO, a composite spatial database derived from upscaling point-based samples, as a means of inferring $S_{bedrock}$. However, we feel comfortable using "soil available water storage" (reported as AWS in the gNATSGO database) to estimate $S_{bedrock}$ for the following reasons: (a) the masking process, as outlined by McCormick et al. (2021), selects for AWS values with a high "likely value" returning the largest likely S_{soil} value, and (b) the deficit-based approach to S_R represents a minimum root-zone storage deficit and therefore would under-estimate the contribution of $S_{bedrock}$ to S_R. Our estimates are not meant

19447973, 2024, 8, Downloaded from https://agupubs.onlinelibrary.wiley.com/doi/10.1029/2023WR036719, Wiley Online Library on [21/08/2024]. See the Terms and Conditions (https://onlinelibrary.wiley.com/terms-and-conditions) on Wiley Online Library for rules of use; OA articles are governed by the applicable Creative Commons License

to represent the absolute value of $S_{bedrock}$, rather, a lower-bound estimate of the contribution of $S_{bedrock}$ to water and energy partitioning. Nevertheless, we additionally report the estimated value of $S_{bedrock(my)}$ under the assumption that S_{soil} is twice the value reported in gNATSGO (Figure S15 in Supporting Information S1; inspired by McCormick et al. (2021) Figure S8 in Supporting Information S1) to highlight the difference in magnitude between $S_{bedrock}$ and S_{soil}. Even after doubling S_{soil}, the mean value of $S_{bedrock(my)}$ is 52.0 mm and increases to a mean (median) value of 119 mm (88.7 mm) after removing pixels where $S_{bedrock(my)}$ cannot be detected.

6. Conclusion

In this study, we introduce a simple and reproducible annual water balance framework for assessing the role of $S_{bedrock(a)}$ on water partitioning within the context of the Budyko framework. We then argue that this method does not accurately represent the extent of subsurface storage dynamics and introduce a modified water balance method that accounts for multi-year deficit accrual. We employ this framework to investigate the timing of evapotranspiration inferred to be sourced from $S_{bedrock(my)}$ and the magnitude of summer latent heat flux produced as a result of access to $S_{bedrock(my)}$. Our findings suggest that, in the western contiguous US: (a) the deficit frequently does not reset annually; (b) $S_{bedrock}$ is necessary to explain plant transpiration very early into the growing season; (c) the proportion of precipitation returning to atmosphere would drastically decrease without access to $S_{bedrock(my)}$; (d) the amount of latent heat flux produced as a result of evapotranspiration sourced from bedrock is substantial during the summer; and (e) the magnitude of evapotranspiration sourced from $S_{bedrock(my)}$ is greater in regions where the deficit does not reset annually. These results confirm that $S_{bedrock}$ plays a key role in the local hydrologic cycle, alters water and energy partitioning properties, and potentially influences the severity and frequency of wildfire and mass die-off events. Further research contributing to the role of $S_{bedrock}$ on the land surface energy balance—for example, extreme temperatures, heat waves, wind patterns, etc.—would prove beneficial in understanding the factors governing tree death and wildfire, an issue that is prevalent across the western US.

Data Availability Statement

Flux data (*ET*, *P*, *PET*, and Q) were obtained from Penman-Monteith-Leuning Evapotranspiration (Y. Zhang et al., 2019), Parameter-elevation Regressions on Independent Slopes Model (C. Daly, 2013), TerraClimate (Abatzoglou et al., 2018), and Catchment Attributes and Meteorology for Large-sample Studies (Newman et al., 2015), respectively. Land cover, soil water storage, and snow cover were obtained from USGS National Land Cover Database (Jin et al., 2019), Gridded National Soil Survey Geographic Database (Survey Staff, 2019), and the National Snow and Ice Data Center (Hall et al., 2016). All data products were analyzed using the Google Earth Engine Python API (Gorelick et al., 2017). Data, figures, and code associated with this manuscript are available publicly on HydroShare (Ehlert et al., 2024).

Acknowledgments
We would like to thank Xue Fang, Dave Barnard, and the anonymous reviewer, as well as Lan Wang-Erlandsson, for their insightful and constructive feedback that helped improve the manuscript. Funding was provided by Simon Fraser University, a Natural Sciences and Engineering Research Council of Canada Discovery grant, and Canadian Foundation for Innovation/British Columbia Knowledge Development Fund held by W. J. Hahm.

References

Abatzoglou, J. T., Dobrowski, S. Z., Parks, S. A., & Hegewisch, K. C. (2018). Terraclimate, a high-resolution global dataset of monthly climate and climatic water balance from 1958–2015. *Scientific Data*, *5*(1), 1–12. https://doi.org/10.1038/sdata.2017.191

Ajami, H., Troch, P. A., Maddock, T., III., Meixner, T., & Eastoe, C. (2011). Quantifying mountain block recharge by means of catchment-scale storage-discharge relationships. *Water Resources Research*, *47*(4), W04504. https://doi.org/10.1029/2010wr009598

Alfieri, L., Claps, P., D'Odorico, P., Laio, F., & Over, T. M. (2008). An analysis of the soil moisture feedback on convective and stratiform precipitation. *Journal of Hydrometeorology*, *9*(2), 280–291. https://doi.org/10.1175/2007jhm863.1

Anderson, M. A., Graham, R. C., Alyanakian, G. J., & Martynn, D. Z. (1995). Late summer water status of soils and weathered bedrock in a giant sequoia grove. *Soil Science*, *160*(6), 415–422. https://doi.org/10.1097/00010694-199512000-00007

Anderson, M. G., & Ferree, C. E. (2010). Conserving the stage: Climate change and the geophysical underpinnings of species diversity. *PLoS One*, *5*(7), e11554. https://doi.org/10.1371/journal.pone.0011554

Anderson, R. S., Anderson, S. P., & Tucker, G. E. (2013). Rock damage and regolith transport by frost: An example of climate modulation of the geomorphology of the critical zone. *Earth Surface Processes and Landforms*, *38*(3), 299–316. https://doi.org/10.1002/esp.3330

Anderson, S. P., Dietrich, W. E., Montgomery, D. R., Torres, R., Conrad, M. E., & Loague, K. (1997). Subsurface flow paths in a steep, unchanneled catchment. *Water Resources Research*, *33*(12), 2637–2653. https://doi.org/10.1029/97wr02595

Arkley, R. J. (1981). Soil moisture use by mixed conifer forest in a summer-dry climate. *Soil Science Society of America Journal*, *45*(2), 423–427. https://doi.org/10.2136/sssaj1981.03615995004500020037x

Awada, H., Di Prima, S., Sirca, C., Giadrossich, F., Marras, S., Spano, D., & Pirastru, M. (2021). Daily actual evapotranspiration estimation in a Mediterranean ecosystem from landsat observations using SEBAL approach. *Forests*, *12*(2), 189. https://doi.org/10.3390/f12020189

Bales, R. C., Molotch, N. P., Painter, T. H., Dettinger, M. D., Rice, R., & Dozier, J. (2006). Mountain hydrology of the western United States. *Water Resources Research*, *42*(8), W08432. https://doi.org/10.1029/2005wr004387

Berghuijs, W. R., Gnann, S. J., & Woods, R. A. (2020). Unanswered questions on the Budyko framework. *Journal of Hydrology*, *265*, 164–177.

Beven, K. (2006). Searching for the holy grail of scientific hydrology: Q t=(s, r, δt) a as closure. *Hydrology and Earth System Sciences*, *10*(5), 609–618. https://doi.org/10.5194/hess-10-609-2006

Brabson, B., Lister, D., Jones, P., & Palutikof, J. (2005). Soil moisture and predicted spells of extreme temperatures in Britain. *Journal of Geophysical Research*, *110*(D5), D05104. https://doi.org/10.1029/2004jd005156

Brantley, S. L. (2010). Rock to regolith. *Nature Geoscience*, *3*(5), 305–306. https://doi.org/10.1038/ngeo858

Brantley, S. L., Lebedeva, M., & Bazilevskaya, E. (2013). Relating weathering fronts for acid neutralization and oxidation to pCO_2 and pO_2. In *The atmosphere-history* (pp. 327–352). Elsevier Inc.

Brantley, S. L., Lebedeva, M. I., Balashov, V. N., Singha, K., Sullivan, P. L., & Stinchcomb, G. (2017). Toward a conceptual model relating chemical reaction fronts to water flow paths in hills. *Geomorphology*, *277*, 100–117. https://doi.org/10.1016/j.geomorph.2016.09.027

Budyko, M. I. (1974). *Climate and life*. Academic Press.

Buss, H. L., Sak, P. B., Webb, S. M., & Brantley, S. L. (2008). Weathering of the Rio Blanco quartz diorite, Luquillo Mountains, Puerto Rico: Coupling oxidation, dissolution, and fracturing. *Geochimica et Cosmochimica Acta*, *72*(18), 4488–4507. https://doi.org/10.1016/j.gca.2008.06.020

Cai, L., Xiong, K., Liu, Z., Li, Y., & Fan, B. (2023). Seasonal variations of plant water use in the karst desertification control. *Science of the Total Environment*, *885*, 163778. https://doi.org/10.1016/j.scitotenv.2023.163778

California Department of Water Resources, C. (2021). Water year 2021: An extreme year. Retrieved from https://water.ca.gov/-/media/DWR-Website/Web-Pages/Water-Basics/Drought/Files/Publications-And-Reports/091521-Water-Year-2021-broch_v2.pdf

Chen, X., Alimohammadi, N., & Wang, D. (2013). Modeling interannual variability of seasonal evaporation and storage change based on the extended Budyko framework. *Water Resources Research*, *49*(9), 6067–6078. https://doi.org/10.1002/wrcr.20493

Cheng, S., Cheng, L., Qin, S., Zhang, L., Liu, P., Liu, L., et al. (2022). Improved understanding of how catchment properties control hydrological partitioning through machine learning. *Water Resources Research*, *58*(4), e2021WR031412. https://doi.org/10.1029/2021wr031412

Choudhury, B. (1999). Evaluation of an empirical equation for annual evaporation using field observations and results from a biophysical model. *Journal of Hydrology*, *216*(1–2), 99–110. https://doi.org/10.1016/s0022-1694(98)00293-5

Condon, L. E., Markovich, K. H., Kelleher, C. A., McDonnell, J. J., Ferguson, G., & McIntosh, J. C. (2020). Where is the bottom of a watershed? *Water Resources Research*, *56*(3), e2019WR026010. https://doi.org/10.1029/2019wr026010

Condon, L. E., & Maxwell, R. M. (2017). Systematic shifts in Budyko relationships caused by groundwater storage changes. *Hydrology and Earth System Sciences*, *21*(2), 1117–1135. https://doi.org/10.5194/hess-21-1117-2017

Cooper, A. E., Kirchner, J. W., Wolf, S., Lombardozzi, D. L., Sullivan, B. W., Tyler, S. W., & Harpold, A. A. (2020). Snowmelt causes different limitations on transpiration in a Sierra Nevada conifer forest. *Agricultural and Forest Meteorology*, *291*, 108089. https://doi.org/10.1016/j.agrformet.2020.108089

Cui, G., Ma, Q., & Bales, R. (2022). Assessing multi-year-drought vulnerability in dense Mediterranean-climate forests using water-balance-based indicators. *Journal of Hydrology*, *606*, 127431. https://doi.org/10.1016/j.jhydrol.2022.127431

Daly, C. (2013). Descriptions of prism spatial climate datasets for the conterminous United States (Vol. *14*). Retrieved from http://www.prism.oregonstate.edu/documents/PRISM_datasets_aug2013.pdf

Daly, C., Halbleib, M., Smith, J. I., Gibson, W. P., Doggett, M. K., Taylor, G. H., et al. (2008). Physiographically sensitive mapping of climatological temperature and precipitation across the conterminous United States. *International Journal of Climatology: A Journal of the Royal Meteorological Society*, *28*(15), 2031–2064. https://doi.org/10.1002/joc.1688

Daly, C., Neilson, R. P., & Phillips, D. L. (1994). A statistical-topographic model for mapping climatological precipitation over mountainous terrain. *Journal of Applied Meteorology and Climatology*, *33*(2), 140–158. https://doi.org/10.1175/1520-0450(1994)033<0140:astmfm>2.0.co;2

Daly, C., Slater, M. E., Roberti, J. A., Laseter, S. H., & Swift Jr, L. W. (2017). High-resolution precipitation mapping in a mountainous watershed: Ground truth for evaluating uncertainty in a national precipitation dataset. *International Journal of Climatology*, *37*(S1), 124–137. https://doi.org/10.1002/joc.4986

Daly, C., Smith, J. I., & Olson, K. V. (2015). Mapping atmospheric moisture climatologies across the conterminous United States. *PLoS One*, *10*(10), e0141140. https://doi.org/10.1371/journal.pone.0141140

Daly, E., Calabrese, S., Yin, J., & Porporato, A. (2019). Hydrological spaces of long-term catchment water balance. *Water Resources Research*, *55*(12), 10747–10764. https://doi.org/10.1029/2019wr025952

Dawson, T. E., Hahm, W. J., & Crutchfield-Peters, K. (2020). Digging deeper: What the critical zone perspective adds to the study of plant ecophysiology. *New Phytologist*, *226*(3), 666–671. https://doi.org/10.1111/nph.16410

de Boer-Euser, T., McMillan, H. K., Hrachowitz, M., Winsemius, H. C., & Savenije, H. H. (2016). Influence of soil and climate on root zone storage capacity. *Water Resources Research*, *52*(3), 2009–2024. https://doi.org/10.1002/2015wr018115

De Lavenne, A., & Andréassian, V. (2018). Impact of climate seasonality on catchment yield: A parameterization for commonly-used water balance formulas. *Journal of Hydrology*, *558*, 266–274. https://doi.org/10.1016/j.jhydrol.2018.01.009

Diffenbaugh, N. S., Pal, J. S., Giorgi, F., & Gao, X. (2007). Heat stress intensification in the Mediterranean climate change hotspot. *Geophysical Research Letters*, *34*(11), L11706. https://doi.org/10.1029/2007gl030000

Donohue, R., Roderick, M., & McVicar, T. R. (2007). On the importance of including vegetation dynamics in Budyko's hydrological model. *Hydrology and Earth System Sciences*, *11*(2), 983–995. https://doi.org/10.5194/hess-11-983-2007

Donohue, R., Roderick, M. L., & McVicar, T. R. (2012). Roots, storms and soil pores: Incorporating key ecohydrological processes into Budyko's hydrological model. *Journal of Hydrology*, *436*, 35–50. https://doi.org/10.1016/j.jhydrol.2012.02.033

Dralle, D. N., Hahm, W. J., Chadwick, K. D., McCormick, E., & Rempe, D. M. (2021). Accounting for snow in the estimation of root zone water storage capacity from precipitation and evapotranspiration fluxes. *Hydrology and Earth System Sciences*, *25*(5), 2861–2867. https://doi.org/10.5194/hess-25-2861-2021

Dralle, D. N., Hahm, W. J., Rempe, D. M., Karst, N., Anderegg, L. D., Thompson, S. E., et al. (2020). Plants as sensors: Vegetation response to rainfall predicts root-zone water storage capacity in Mediterranean-type climates. *Environmental Research Letters*, *15*(10), 104074. https://doi.org/10.1088/1748-9326/abb10b

Dralle, D. N., Hahm, W. J., Rempe, D. M., Karst, N. J., Thompson, S. E., & Dietrich, W. E. (2018). Quantification of the seasonal hillslope water storage that does not drive streamflow. *Hydrological Processes*, *32*(13), 1978–1992. https://doi.org/10.1002/hyp.11627

Dubovik, O., Schuster, G. L., Xu, F., Hu, Y., Bösch, H., Landgraf, J., & Li, Z. (2021). *Grand challenges in satellite remote sensing* (Vol. 2). Frontiers Media SA. https://doi.org/10.3389/frsen.2021.619818

Durre, I., Wallace, J. M., & Lettenmaier, D. P. (2000). Dependence of extreme daily maximum temperatures on antecedent soil moisture in the contiguous United States during summer. *Journal of Climate*, *13*(14), 2641–2651. https://doi.org/10.1175/1520-0442(2000)013<2641:doedmt>2.0.co;2

19447973, 2024, 8, Downloaded from https://agupubs.onlinelibrary.wiley.com/doi/10.1029/2023WR036719, Wiley Online Library on [21/08/2024]. See the Terms and Conditions (https://onlinelibrary.wiley.com/terms-and-conditions) on Wiley Online Library for rules of use; OA articles are governed by the applicable Creative Commons License

Ehlert, R., Hahm, J. W., Dralle, D., Rempe, D. M., & Allen, D. M. (2024). Bedrock controls on water and energy partitioning [Dataset and Code]. *HydroShare*. https://doi.org/10.4211/hs.0fa38cceb83344909bd51d3d0fec4fc8

Ek, M., & Holtslag, A. (2004). Influence of soil moisture on boundary layer cloud development. *Journal of Hydrometeorology*, *5*(1), 86–99. https://doi.org/10.1175/1525-7541(2004)005<0086:iosmob>2.0.co;2

Entekhabi, D., & Rodriguez-Iturbe, I. (1994). Analytical framework for the characterization of the space-time variability of soil moisture. *Advances in Water Resources*, *17*(1–2), 35–45. https://doi.org/10.1016/0309-1708(94)90022-1

Fan, Y. (2019). Are catchments leaky? *Wiley Interdisciplinary Reviews: Water*, *6*(6), e1386. https://doi.org/10.1002/wat2.1386

Feng, X., Porporato, A., & Rodriguez-Iturbe, I. (2015). Stochastic soil water balance under seasonal climates. *Proceedings of the Royal Society A: Mathematical, Physical and Engineering Sciences*, *471*(2174), 20140623. https://doi.org/10.1098/rspa.2014.0623

Feng, X., Thompson, S. E., Woods, R., & Porporato, A. (2019). Quantifying asynchronicity of precipitation and potential evapotranspiration in Mediterranean climates. *Geophysical Research Letters*, *46*(24), 14692–14701. https://doi.org/10.1029/2019gl085653

Feng, X., Vico, G., & Porporato, A. (2012). On the effects of seasonality on soil water balance and plant growth. *Water Resources Research*, *48*(5), W05543. https://doi.org/10.1029/2011wr011263

Finch, J. (2001). Estimating change in direct groundwater recharge using a spatially distributed soil water balance model. *The Quarterly Journal of Engineering Geology and Hydrogeology*, *34*(1), 71–83. https://doi.org/10.1144/qjegh.34.1.71

Finlay, R. D., Mahmood, S., Rosenstock, N., Bolou-Bi, E. B., Köhler, S. J., Fahad, Z., et al. (2020). Reviews and syntheses: Biological weathering and its consequences at different spatial levels–from nanoscale to global scale. *Biogeosciences*, *17*(6), 1507–1533. https://doi.org/10.5194/bg-17-1507-2020

Fischer, E. M., Seneviratne, S. I., Vidale, P. L., Lüthi, D., & Schär, C. (2007). Soil moisture–atmosphere interactions during the 2003 European summer heat wave. *Journal of Climate*, *20*(20), 5081–5099. https://doi.org/10.1175/jcli4288.1

Fu, B. (1981). On the calculation of the evaporation from land surface. *Scientia Atmospherica Sinica*, *5*(1), 23.

Fu, J., & Wang, W. (2019). On the lower bound of Budyko curve: The influence of precipitation seasonality. *Journal of Hydrology*, *570*, 292–303. https://doi.org/10.1016/j.jhydrol.2018.12.062

Gao, H., Hrachowitz, M., Schymanski, S., Fenicia, F., Sriwongsitanon, N., & Savenije, H. (2014). Climate controls how ecosystems size the root zone storage capacity at catchment scale. *Geophysical Research Letters*, *41*(22), 7916–7923. https://doi.org/10.1002/2014gl061668

Gentine, P., D'Odorico, P., Lintner, B. R., Sivandran, G., & Salvucci, G. (2012). Interdependence of climate, soil, and vegetation as constrained by the Budyko curve. *Geophysical Research Letters*, *39*(19), L19404. https://doi.org/10.1029/2012gl053492

Gerrits, A., Savenije, H., Veling, E., & Pfister, L. (2009). Analytical derivation of the Budyko curve based on rainfall characteristics and a simple evaporation model. *Water Resources Research*, *45*(4), W04403. https://doi.org/10.1029/2008wr007308

Gorelick, N., Hancher, M., Dixon, M., Ilyushchenko, S., Thau, D., & Moore, R. (2017). Google Earth engine: Planetary-scale geospatial analysis for everyone. *Remote Sensing of Environment*, *202*, 18–27. https://doi.org/10.1016/j.rse.2017.06.031

Goulden, M. L., & Bales, R. C. (2019). California forest die-off linked to multi-year deep soil drying in 2012–2015 drought. *Nature Geoscience*, *12*(8), 632–637. https://doi.org/10.1038/s41561-019-0388-5

Graham, R., Rossi, A., & Hubbert, R. (2010). Rock to regolith conversion: Producing hospitable substrates for terrestrial ecosystems. *Geological Society of America Today*, *20*, 4–9. https://doi.org/10.1130/gsat57a.1

Grindley, J. (1960). Calculated soil moisture deficits in the dry summer of 1959 and forecast dates of first appreciable runoff. *International Association of Scientific Hydrology*, 109–120.

Grindley, J. (1968). The estimation of soil moisture deficits. *Water for Peace: Water Supply Technology*, *3*, 241.

Haarsma, R. J., Selten, F., Hurk, B. V., Hazeleger, W., & Wang, X. (2009). Drier Mediterranean soils due to greenhouse warming bring easterly winds over summertime central Europe. *Geophysical Research Letters*, *36*(4), L04705. https://doi.org/10.1029/2008gl036617

Hahm, W. J., Dralle, D., Lapides, D., Ehlert, R., & Rempe, D. (2024). Geologic controls on apparent root-zone storage capacity. *Water Resources Research*, *60*(3), e2023WR035362. https://doi.org/10.1029/2023wr035362

Hahm, W. J., Dralle, D. N., Sanders, M., Bryk, A. B., Fauria, K. E., Huang, M.-H., et al. (2022). Bedrock vadose zone storage dynamics under extreme drought: Consequences for plant water availability, recharge, and runoff. *Water Resources Research*, *58*(4), e2021WR031781. https://doi.org/10.1029/2021wr031781

Hahm, W. J., Rempe, D., Dralle, D., Dawson, T., & Dietrich, W. (2020). Oak transpiration drawn from the weathered bedrock vadose zone in the summer dry season. *Water Resources Research*, *56*(11), e2020WR027419. https://doi.org/10.1029/2020wr027419

Hahm, W. J., Rempe, D. M., Dralle, D. N., Dawson, T. E., Lovill, S. M., Bryk, A. B., et al. (2019). Lithologically controlled subsurface critical zone thickness and water storage capacity determine regional plant community composition. *Water Resources Research*, *55*(4), 3028–3055. https://doi.org/10.1029/2018wr023760

Hahm, W. J., Riebe, C. S., Lukens, C. E., & Araki, S. (2014). Bedrock composition regulates mountain ecosystems and landscape evolution. *Proceedings of the National Academy of Sciences of the United States of America*, *111*(9), 3338–3343. https://doi.org/10.1073/pnas.1315667111

Hall, D., Riggs, G., & Salomonson, V. (2016). MODIS/terra snow cover daily L3 global 500m grid, version 6. Retrieved from https://nsidc.org/data/myd10a1/versions/6

Hasenmueller, E. A., Gu, X., Weitzman, J. N., Adams, T. S., Stinchcomb, G. E., Eissenstat, D. M., et al. (2017). Weathering of rock to regolith: The activity of deep roots in bedrock fractures. *Geoderma*, *300*, 11–31. https://doi.org/10.1016/j.geoderma.2017.03.020

He, S., Zhang, Y., Ma, N., Tian, J., Kong, D., & Liu, C. (2022). A daily and 500 m coupled evapotranspiration and gross primary production product across China during 2000–2020. *Earth System Science Data Discussions*, *2022*(12), 1–42. https://doi.org/10.5194/essd-14-5463-2022

Henn, B., Newman, A. J., Livneh, B., Daly, C., & Lundquist, J. D. (2018). An assessment of differences in gridded precipitation datasets in complex terrain. *Journal of Hydrology*, *556*, 1205–1219. https://doi.org/10.1016/j.jhydrol.2017.03.008

Hickel, K., & Zhang, L. (2006). Estimating the impact of rainfall seasonality on mean annual water balance using a top-down approach. *Journal of Hydrology*, *331*(3–4), 409–424. https://doi.org/10.1016/j.jhydrol.2006.05.028

Hickler, T., Prentice, I. C., Smith, B., Sykes, M. T., & Zaehle, S. (2006). Implementing plant hydraulic architecture within the LPJ dynamic global vegetation model. *Global Ecology and Biogeography*, *15*(6), 567–577. https://doi.org/10.1111/j.1466-8238.2006.00254.x

Hickler, T., Vohland, K., Feehan, J., Miller, P. A., Smith, B., Costa, L., et al. (2012). Projecting the future distribution of European potential natural vegetation zones with a generalized, tree species-based dynamic vegetation model. *Global Ecology and Biogeography*, *21*(1), 50–63. https://doi.org/10.1111/j.1466-8238.2010.00613.x

Hubbert, K., Beyers, J., & Graham, R. (2001). Roles of weathered bedrock and soil in seasonal water relations of *Pinus jeffreyi* and *Arctostaphylos patula*. *Canadian Journal of Forest Research*, *31*(11), 1947–1957. https://doi.org/10.1139/x01-136

19447973, 2024, 8, Downloaded from https://agupubs.onlinelibrary.wiley.com/doi/10.1029/2023WR036719, Wiley Online Library on [21/08/2024]. See the Terms and Conditions (https://onlinelibrary.wiley.com/terms-and-conditions) on Wiley Online Library for rules of use; OA articles are governed by the applicable Creative Commons License

Janssens, I. A., Lankreijer, H., Matteucci, G., Kowalski, A., Buchmann, N., Epron, D., et al. (2001). Productivity overshadows temperature in determining soil and ecosystem respiration across European forests. *Global Change Biology*, *7*(3), 269–278. https://doi.org/10.1046/j.1365-2486.2001.00412.x

Jasechko, S., Sharp, Z. D., Gibson, J. J., Birks, S. J., Yi, Y., & Fawcett, P. J. (2013). Terrestrial water fluxes dominated by transpiration. *Nature*, *496*(7445), 347–350. https://doi.org/10.1038/nature11983

Jensen, D., Reager, J. T., Zajic, B., Rousseau, N., Rodell, M., & Hinkley, E. (2018). The sensitivity of us wildfire occurrence to pre-season soil moisture conditions across ecosystems. *Environmental Research Letters*, *13*(1), 014021. https://doi.org/10.1088/1748-9326/aa9853

Ji, Y., Tang, Q., Yan, L., Wu, S., Yan, L., Tan, D., et al. (2021). Spatiotemporal variations and influencing factors of terrestrial evapotranspiration and its components during different impoundment periods in the three gorges reservoir area. *Water*, *13*(15), 2111. https://doi.org/10.3390/w13152111

Jiang, Z., Liu, H., Wang, H., Peng, J., Meersmans, J., Green, S. M., et al. (2020). Bedrock geochemistry influences vegetation growth by regulating the regolith water holding capacity. *Nature Communications*, *11*(1), 2392. https://doi.org/10.1038/s41467-020-16156-1

Jin, S., Homer, C., Yang, L., Danielson, P., Dewitz, J., Li, C., et al. (2019). Overall methodology design for the United States national land cover database 2016 products. *Remote Sensing*, *11*(24), 2971. https://doi.org/10.3390/rs11242971

Johnson, B., & Goldblatt, C. (2015). The nitrogen budget of Earth. *Earth-Science Reviews*, *148*, 150–173. https://doi.org/10.1016/j.earscirev.2015.05.006

Jones, D., & Graham, R. (1993). Water-holding characteristics of weathered granitic rock in chaparral and forest ecosystems. *Soil Science Society of America Journal*, *57*(1), 256–261. https://doi.org/10.2136/sssaj1993.03615995005700010044x

Kelly, A. E., & Goulden, M. L. (2016). A montane Mediterranean climate supports year-round photosynthesis and high forest biomass. *Tree Physiology*, *36*(4), 459–468. https://doi.org/10.1093/treephys/tpv131

Kim, H., Dietrich, W. E., Thurnhoffer, B. M., Bishop, J. K., & Fung, I. Y. (2017). Controls on solute concentration-discharge relationships revealed by simultaneous hydrochemistry observations of hillslope runoff and stream flow: The importance of critical zone structure. *Water Resources Research*, *53*(2), 1424–1443. https://doi.org/10.1002/2016wr019722

Klos, P. Z., Goulden, M. L., Riebe, C. S., Tague, C. L., O'Geen, A. T., Flinchum, B. A., et al. (2018). Subsurface plant-accessible water in mountain ecosystems with a Mediterranean climate. *Wiley Interdisciplinary Reviews: Water*, *5*(3), e1277. https://doi.org/10.1002/wat2.1277

Koster, R. D., Dirmeyer, P. A., Guo, Z., Bonan, G., Chan, E., Cox, P., et al. (2004). Regions of strong coupling between soil moisture and precipitation. *Science*, *305*(5687), 1138–1140. https://doi.org/10.1126/science.1100217

Kottek, M., Grieser, J., Beck, C., Rudolf, B., & Rubel, F. (2006). World map of the Köppen-Geiger climate classification updated.

Kraft, M., & McNamara, J. P. (2022). Evapotranspiration across the rain–snow transition in a semi-arid watershed. *Hydrological Processes*, *36*(3), e14519. https://doi.org/10.1002/hyp.14519

Kruckeberg, A. (1992). Plant life of western North American ultramafics. In *The ecology of areas with serpentinized rocks: a world view* (pp. 31–73). https://doi.org/10.1007/978-94-011-3722-5_3

Kunkel, K. E., Karl, T. R., Brooks, H., Kossin, J., Lawrimore, J. H., Arndt, D., et al. (2013). Monitoring and understanding trends in extreme storms: State of knowledge. *Bulletin of the American Meteorological Society*, *94*(4), 499–514. https://doi.org/10.1175/bams-d-11-00262.1

Lapides, D. A., Hahm, W. J., Forrest, M., Rempe, D. M., Hickler, T., & Dralle, D. N. (2024). Inclusion of bedrock vadose zone in dynamic global vegetation models is key for simulating vegetation structure and function. *Biogeosciences*, *21*(7), 1801–1826. https://doi.org/10.5194/bg-21-1801-2024

Lapides, D. A., Hahm, W. J., Rempe, D. M., Dietrich, W. E., & Dralle, D. N. (2022). Controls on stream water age in a saturation overland flow-dominated catchment. *Water Resources Research*, *58*(4), e2021WR031665. https://doi.org/10.1029/2021wr031665

Lapides, D. A., Hahm, W. J., Rempe, D. M., Whiting, J., & Dralle, D. N. (2022). Causes of missing snowmelt following drought. *Geophysical Research Letters*, *49*(19), e2022GL100505. https://doi.org/10.1029/2022gl100505

Lebedeva, M. I., & Brantley, S. L. (2013). Exploring geochemical controls on weathering and erosion of convex hillslopes: Beyond the empirical regolith production function. *Earth Surface Processes and Landforms*, *38*(15), 1793–1807. https://doi.org/10.1002/esp.3424

Lebedeva, M. I., Fletcher, R. C., Balashov, V., & Brantley, S. L. (2007). A reactive diffusion model describing transformation of bedrock to saprolite. *Chemical Geology*, *244*(3–4), 624–645. https://doi.org/10.1016/j.chemgeo.2007.07.008

Lhomme, J.-P., & Moussa, R. (2016). Matching the Budyko functions with the complementary evaporation relationship: Consequences for the drying power of the air and the Priestley–Taylor coefficient. *Hydrology and Earth System Sciences*, *20*(12), 4857–4865. https://doi.org/10.5194/hess-20-4857-2016

Liu, H., Dai, J., Xu, C., Peng, J., Wu, X., & Wang, H. (2021). Bedrock-associated belowground and aboveground interactions and their implications for vegetation restoration in the karst critical zone of subtropical southwest China. *Progress in Physical Geography: Earth and Environment*, *45*(1), 7–19. https://doi.org/10.1177/0309133320949865

Liu, M., Lin, K., & Cai, X. (2022). Climate and vegetation seasonality play comparable roles in water partitioning within the Budyko framework. *Journal of Hydrology*, *605*, 127373. https://doi.org/10.1016/j.jhydrol.2021.127373

Lundquist, J. D., & Cayan, D. R. (2007). Surface temperature patterns in complex terrain: Daily variations and long-term change in the central Sierra Nevada, California. *Journal of Geophysical Research*, *112*(D11), D11124. https://doi.org/10.1029/2006jd007561

Manning, A. H., Verplanck, P. L., Caine, J. S., & Todd, A. S. (2013). Links between climate change, water-table depth, and water chemistry in a mineralized mountain watershed. *Applied Geochemistry*, *37*, 64–78. https://doi.org/10.1016/j.apgeochem.2013.07.002

McCormick, E. L., Dralle, D. N., Hahm, W. J., Tune, A. K., Schmidt, L. M., Chadwick, K. D., & Rempe, D. M. (2021). Widespread woody plant use of water stored in bedrock. *Nature*, *597*(7875), 225–229. https://doi.org/10.1038/s41586-021-03761-3

McDonnell, J. J., Spence, C., Karran, D. J., Van Meerveld, H., & Harman, C. J. (2021). Fill-and-spill: A process description of runoff generation at the scale of the beholder. *Water Resources Research*, *57*(5), e2020WR027514. https://doi.org/10.1029/2020wr027514

Miller, J. D., Collins, B. M., Lutz, J. A., Stephens, S. L., Van Wagtendonk, J. W., & Yasuda, D. A. (2012). Differences in wildfires among ecoregions and land management agencies in the Sierra Nevada region, California, USA. *Ecosphere*, *3*(9), 1–20. https://doi.org/10.1890/es12-00158.1

Milly, P. (1994a). Climate, interseasonal storage of soil water, and the annual water balance. *Advances in Water Resources*, *17*(1–2), 19–24. https://doi.org/10.1016/0309-1708(94)90020-5

Milly, P. (1994b). Climate, soil water storage, and the average annual water balance. *Water Resources Research*, *30*(7), 2143–2156. https://doi.org/10.1029/94wr00586

Morford, S. L., Houlton, B. Z., & Dahlgren, R. A. (2016). Direct quantification of long-term rock nitrogen inputs to temperate forest ecosystems. *Ecology*, *97*(1), 54–64. https://doi.org/10.1890/15-0501.1

19447973, 2024, 8, Downloaded from https://agupubs.onlinelibrary.wiley.com/doi/10.1029/2023WR036719, Wiley Online Library on [21/08/2024]. See the Terms and Conditions (https://onlinelibrary.wiley.com/terms-and-conditions) on Wiley Online Library for rules of use; OA articles are governed by the applicable Creative Commons License

Newman, A. J., Clark, M. P., Sampson, K., Wood, A., Hay, L. E., Bock, A., et al. (2015). Development of a large-sample watershed-scale hydrometeorological data set for the contiguous USA: Data set characteristics and assessment of regional variability in hydrologic model performance. *Hydrology and Earth System Sciences*, *19*(1), 209–223. https://doi.org/10.5194/hess-19-209-2015

Nimmo, J. R. (2021). The processes of preferential flow in the unsaturated zone. *Soil Science Society of America Journal*, *85*(1), 1–27. https://doi.org/10.1002/saj2.20143

O'Geen, A., Safeeq, M., Wagenbrenner, J., Stacy, E., Hartsough, P., Devine, S., et al. (2018). Southern Sierra critical zone observatory and Kings River experimental watersheds: A synthesis of measurements, new insights, and future directions. *Vadose Zone Journal*, *17*(1), 1–18. https://doi.org/10.2136/vzj2018.04.0081

Ookouchi, Y., Segal, M., Kessler, R., & Pielke, R. (1984). Evaluation of soil moisture effects on the generation and modification of mesoscale circulations. *Monthly Weather Review*, *112*(11), 2281–2292. https://doi.org/10.1175/1520-0493(1984)112<2281:eosmeo>2.0.co;2

Padrón, R. S., Gudmundsson, L., Greve, P., & Seneviratne, S. I. (2017). Large-scale controls of the surface water balance over land: Insights from a systematic review and meta-analysis. *Water Resources Research*, *53*(11), 9659–9678. https://doi.org/10.1002/2017wr021215

Pawlik, Ł., Phillips, J. D., & Šamonil, P. (2016). Roots, rock, and regolith: Biomechanical and biochemical weathering by trees and its impact on hillslopes—A critical literature review. *Earth-Science Reviews*, *159*, 142–159. https://doi.org/10.1016/j.earscirev.2016.06.002

Porporato, A., Daly, E., & Rodriguez-Iturbe, I. (2004). Soil water balance and ecosystem response to climate change. *The American Naturalist*, *164*(5), 625–632. https://doi.org/10.2307/3473173

Potter, N., Zhang, L., Milly, P., McMahon, T. A., & Jakeman, A. (2005). Effects of rainfall seasonality and soil moisture capacity on mean annual water balance for Australian catchments. *Water Resources Research*, *41*(6), W06007. https://doi.org/10.1029/2004wr003697

Rakhmatulina, E., Stephens, S., & Thompson, S. (2021). Soil moisture influences on Sierra Nevada dead fuel moisture content and fire risks. *Forest Ecology and Management*, *496*, 119379. https://doi.org/10.1016/j.foreco.2021.119379

Rempe, D. M., & Dietrich, W. E. (2014). A bottom-up control on fresh-bedrock topography under landscapes. *Proceedings of the National Academy of Sciences of the United States of America*, *111*(18), 6576–6581. https://doi.org/10.1073/pnas.1404763111

Rempe, D. M., & Dietrich, W. E. (2018). Direct observations of rock moisture, a hidden component of the hydrologic cycle. *Proceedings of the National Academy of Sciences of the United States of America*, *115*(11), 2664–2669. https://doi.org/10.1073/pnas.1800141115

Rempe, D. M., McCormick, E. L., Hahm, W. J., Persad, G. G., Cummins, C., Lapides, D. A., et al. (2022). Resilience of woody ecosystems to precipitation variability.

Riebe, C. S., Hahm, W. J., & Brantley, S. L. (2017). Controls on deep critical zone architecture: A historical review and four testable hypotheses. *Earth Surface Processes and Landforms*, *42*(1), 128–156. https://doi.org/10.1002/esp.4052

Rodriguez-Iturbe, I., Porporato, A., Ridolfi, L., Isham, V., & Coxi, D. (1999). Probabilistic modelling of water balance at a point: The role of climate, soil and vegetation. *Proceedings of the Royal Society of London. Series A: Mathematical, Physical and Engineering Sciences*, *455*(1990), 3789–3805. https://doi.org/10.1098/rspa.1999.0477

Rose, K., Graham, R., & Parker, D. (2003). Water source utilization by *Pinus jeffreyi* and *Arctostaphylos patula* on thin soils over bedrock. *Oecologia*, *134*(1), 46–54. https://doi.org/10.1007/s00442-002-1084-4

Rushton, K., Eilers, V., & Carter, R. (2006). Improved soil moisture balance methodology for recharge estimation. *Journal of Hydrology*, *318*(1–4), 379–399. https://doi.org/10.1016/j.jhydrol.2005.06.022

Rushton, K., & Ward, C. (1979). The estimation of groundwater recharge. *Journal of Hydrology*, *41*(3–4), 345–361. https://doi.org/10.1016/0022-1694(79)90070-2

Safeeq, M., Bart, R. R., Pelak, N. F., Singh, C. K., Dralle, D. N., Hartsough, P., & Wagenbrenner, J. W. (2021). How realistic are water-balance closure assumptions? A demonstration from the southern sierra critical zone observatory and Kings River experimental watersheds. *Hydrological Processes*, *35*(5), e14199. https://doi.org/10.1002/hyp.14199

Salve, R., Rempe, D. M., & Dietrich, W. E. (2012). Rain, rock moisture dynamics, and the rapid response of perched groundwater in weathered, fractured argillite underlying a steep hillslope. *Water Resources Research*, *48*(11), W11528. https://doi.org/10.1029/2012wr012583

Sayama, T., McDonnell, J. J., Dhakal, A., & Sullivan, K. (2011). How much water can a watershed store? *Hydrological Processes*, *25*(25), 3899–3908. https://doi.org/10.1002/hyp.8288

Schimel, D. S. (1995). Terrestrial ecosystems and the carbon cycle. *Global Change Biology*, *1*(1), 77–91. https://doi.org/10.1111/j.1365-2486.1995.tb00008.x

Seneviratne, S. I., Lüthi, D., Litschi, M., & Schär, C. (2006). Land–atmosphere coupling and climate change in Europe. *Nature*, *443*(7108), 205–209. https://doi.org/10.1038/nature05095

Singh, C., van der Ent, R., Wang-Erlandsson, L., & Fetzer, I. (2022). Hydroclimatic adaptation critical to the resilience of tropical forests. *Global Change Biology*, *28*(9), 2930–2939. https://doi.org/10.1111/gcb.16115

Singh, C., Wang-Erlandsson, L., Fetzer, I., Rockström, J., & Van Der Ent, R. (2020). Rootzone storage capacity reveals drought coping strategies along rainforest-savanna transitions. *Environmental Research Letters*, *15*(12), 124021. https://doi.org/10.1088/1748-9326/abc377

Sivandran, G., & Bras, R. L. (2013). Dynamic root distributions in ecohydrological modeling: A case study at walnut gulch experimental watershed. *Water Resources Research*, *49*(6), 3292–3305. https://doi.org/10.1002/wrcr.20245

Slim, M., Perron, J. T., Martel, S. J., & Singha, K. (2015). Topographic stress and rock fracture: A two-dimensional numerical model for arbitrary topography and preliminary comparison with borehole observations. *Earth Surface Processes and Landforms*, *40*(4), 512–529. https://doi.org/10.1002/esp.3646

Soulet, G., Hilton, R. G., Garnett, M. H., Roylands, T., Klotz, S., Croissant, T., et al. (2021). Temperature control on CO_2 emissions from the weathering of sedimentary rocks. *Nature Geoscience*, *14*(9), 665–671. https://doi.org/10.1038/s41561-021-00805-1

Sousa, P. M., Barriopedro, D., García-Herrera, R., Ordóñez, C., Soares, P. M., & Trigo, R. M. (2020). Distinct influences of large-scale circulation and regional feedbacks in two exceptional 2019 European heatwaves. *Communications Earth & Environment*, *1*(1), 48. https://doi.org/10.1038/s43247-020-00048-9

Sposito, G. (2017). Incorporating the vadose zone into the Budyko framework. *Water*, *9*(9), 698. https://doi.org/10.3390/w9090698

St. Clair, J., Moon, S., Holbrook, W., Perron, J., Riebe, C., Martel, S., et al. (2015). Geophysical imaging reveals topographic stress control of bedrock weathering. *Science*, *350*(6260), 534–538. https://doi.org/10.1126/science.aab2210

Stocker, B. D., Tumber-Dávila, S. J., Konings, A. G., Anderson, M. C., Hain, C., & Jackson, R. B. (2023). Global patterns of water storage in the rooting zones of vegetation. *Nature Geoscience*, *16*(3), 250–256. https://doi.org/10.1038/s41561-023-01125-2

Strachan, S., & Daly, C. (2017). Testing the daily prism air temperature model on semiarid mountain slopes. *Journal of Geophysical Research: Atmospheres*, *122*(11), 5697–5715. https://doi.org/10.1002/2016jd025920

Survey Staff, S. (2019). *Gridded national soil survey geographic (gNATSGO) database for the conterminous United States*. United States Department of Agriculture, Natural Resources Conservation Service. Retrieved from https://nrcs.app.box.com/v/soils

19447973, 2024, 8, Downloaded from https://agupubs.onlinelibrary.wiley.com/doi/10.1029/2023WR036719, Wiley Online Library on [21/08/2024]. See the Terms and Conditions (https://onlinelibrary.wiley.com/terms-and-conditions) on Wiley Online Library for rules of use; OA articles are governed by the applicable Creative Commons License

Tao, S., Song, L., Zhao, G., & Zhao, L. (2024). Simulation and assessment of daily evapotranspiration in the Heihe river basin over a long time series based on TSEB-SM. *Remote Sensing*, *16*(3), 462. https://doi.org/10.3390/rs16030462

Taylor, C. M. (2015). Detecting soil moisture impacts on convective initiation in Europe. *Geophysical Research Letters*, *42*(11), 4631–4638. https://doi.org/10.1002/2015gl064030

Torres, M. A., West, A. J., & Clark, K. E. (2015). Geomorphic regime modulates hydrologic control of chemical weathering in the andes–amazon. *Geochimica et Cosmochimica Acta*, *166*, 105–128. https://doi.org/10.1016/j.gca.2015.06.007

Trenberth, K. E., Smith, L., Qian, T., Dai, A., & Fasullo, J. (2007). Estimates of the global water budget and its annual cycle using observational and model data. *Journal of Hydrometeorology*, *8*(4), 758–769. https://doi.org/10.1175/jhm600.1

Tromp-van Meerveld, H., Peters, N., & McDonnell, J. (2007). Effect of bedrock permeability on subsurface stormflow and the water balance of a trenched hillslope at the Panola Mountain Research Watershed, Georgia, USA. *Hydrological Processes: An International Journal*, *21*(6), 750–769. https://doi.org/10.1002/hyp.6265

Tsaknias, D., Bouziotas, D., & Koutsoyiannis, D. (2016). Statistical comparison of observed temperature and rainfall extremes with climate model outputs in the Mediterranean region. *ResearchGate*, *10*.

Tune, A. K., Druhan, J. L., Wang, J., Bennett, P. C., & Rempe, D. M. (2020). Carbon dioxide production in bedrock beneath soils substantially contributes to forest carbon cycling. *Journal of Geophysical Research: Biogeosciences*, *125*(12), e2020JG005795. https://doi.org/10.1029/2020jg005795

Viola, F., Caracciolo, D., Forestieri, A., Pumo, D., & Noto, L. (2017). Annual runoff assessment in arid and semiarid Mediterranean watersheds under the Budyko's framework. *Hydrological Processes*, *31*(10), 1876–1888. https://doi.org/10.1002/hyp.11145

Wan, J., Tokunaga, T. K., Brown, W., Newman, A. W., Dong, W., Bill, M., et al. (2021). Bedrock weathering contributes to subsurface reactive nitrogen and nitrous oxide emissions. *Nature Geoscience*, *14*(4), 217–224. https://doi.org/10.1038/s41561-021-00717-0

Wang, X.-S., & Zhou, Y. (2016). Shift of annual water balance in the Budyko space for catchments with groundwater-dependent evapotranspiration. *Hydrology and Earth System Sciences*, *20*(9), 3673–3690. https://doi.org/10.5194/hess-20-3673-2016

Wang-Erlandsson, L., Bastiaanssen, W. G., Gao, H., Jägermeyr, J., Senay, G. B., Van Dijk, A. I., et al. (2016). Global root zone storage capacity from satellite-based evaporation. *Hydrology and Earth System Sciences*, *20*(4), 1459–1481. https://doi.org/10.5194/hess-20-1459-2016

Williams, C. A., Reichstein, M., Buchmann, N., Baldocchi, D., Beer, C., Schwalm, C., et al. (2012). Climate and vegetation controls on the surface water balance: Synthesis of evapotranspiration measured across a global network of flux towers. *Water Resources Research*, *48*(6), W06523. https://doi.org/10.1029/2011wr011586

Winnick, M. J., Carroll, R. W., Williams, K. H., Maxwell, R. M., Dong, W., & Maher, K. (2017). Snowmelt controls on concentration-discharge relationships and the balance of oxidative and acid-base weathering fluxes in an alpine catchment, East River, Colorado. *Water Resources Research*, *53*(3), 2507–2523. https://doi.org/10.1002/2016wr019724

Witty, J. H., Graham, R. C., Hubbert, K. R., Doolittle, J. A., & Wald, J. A. (2003). Contributions of water supply from the weathered bedrock zone to forest soil quality. *Geoderma*, *114*(3–4), 389–400. https://doi.org/10.1016/s0016-7061(03)00051-x

Woods, R. (2003). The relative roles of climate, soil, vegetation and topography in determining seasonal and long-term catchment dynamics. *Advances in Water Resources*, *26*(3), 295–309. https://doi.org/10.1016/s0309-1708(02)00164-1

Xing, W., Wang, W., Shao, Q., & Yong, B. (2018). Identification of dominant interactions between climatic seasonality, catchment characteristics and agricultural activities on Budyko-type equation parameter estimation. *Journal of Hydrology*, *556*, 585–599. https://doi.org/10.1016/j.jhydrol.2017.11.048

Yang, H., Qi, J., Xu, X., Yang, D., & Lv, H. (2014). The regional variation in climate elasticity and climate contribution to runoff across China. *Journal of Hydrology*, *517*, 607–616. https://doi.org/10.1016/j.jhydrol.2014.05.062

Yang, H., Yang, D., Lei, Z., & Sun, F. (2008). New analytical derivation of the mean annual water-energy balance equation. *Water Resources Research*, *44*(3), W03410. https://doi.org/10.1029/2007wr006135

Yang, L., Jin, S., Danielson, P., Homer, C., Gass, L., Bender, S. M., et al. (2018). A new generation of the United States national land cover database: Requirements, research priorities, design, and implementation strategies. *ISPRS Journal of Photogrammetry and Remote Sensing*, *146*, 108–123. https://doi.org/10.1016/j.isprsjprs.2018.09.006

Yokoo, Y., Sivapalan, M., & Oki, T. (2008). Investigating the roles of climate seasonality and landscape characteristics on mean annual and monthly water balances. *Journal of Hydrology*, *357*(3–4), 255–269. https://doi.org/10.1016/j.jhydrol.2008.05.010

Zanner, C. W., & Graham, R. C. (2005). Deep regolith: Exploring the lower reaches of soil. *Geoderma*, *1*(126), 1–3. https://doi.org/10.1016/j.geoderma.2004.11.004

Zhang, L., Dawes, W., & Walker, G. (2001). Response of mean annual evapotranspiration to vegetation changes at catchment scale. *Water Resources Research*, *37*(3), 701–708. https://doi.org/10.1029/2000wr900325

Zhang, Y., Kong, D., Gan, R., Chiew, F. H., McVicar, T. R., Zhang, Q., & Yang, Y. (2019). Coupled estimation of 500 m and 8-day resolution global evapotranspiration and gross primary production in 2002–2017. *Remote Sensing of Environment*, *222*, 165–182. https://doi.org/10.1016/j.rse.2018.12.031

References From the Supporting Information

Running, S. W., Mu, Q., Zhao, M., & Moreno, A. (2017). *Modis global terrestrial evapotranspiration (ET) product (NASA MOD16A2/A3) NASA Earth observing system MODIS land algorithm*. NASA.

19447973, 2024, 8, Downloaded from https://agupubs.onlinelibrary.wiley.com/doi/10.1029/2023WR036719, Wiley Online Library on [21/08/2024]. See the Terms and Conditions (https://onlinelibrary.wiley.com/terms-and-conditions) on Wiley Online Library for rules of use; OA articles are governed by the applicable Creative Commons License